A novel Visbreaking-Supercritical Fluid extraction (SFE) strategy for efficient upgrading of vacuum residue

Experimental optimization and molecular dynamics insights

Ren, Shisong; He, Ying; Liu, Cheng; Fan, Weiyu; Van den bergh, Wim; Varveri, Aikaterini

DOI
10.1016/j.seppur.2025.133554

Publication date
2025

Document Version
Final published version

Published in
Separation and Purification Technology

Citation (APA)
Ren, S., He, Y., Liu, C., Fan, W., Van den bergh, W., & Varveri, A. (2025). A novel Visbreaking-Supercritical Fluid extraction (SFE) strategy for efficient upgrading of vacuum residue: Experimental optimization and molecular dynamics insights. *Separation and Purification Technology*, *373*, Article 133554. https://doi.org/10.1016/j.seppur.2025.133554

Separation and Purification Technology 373 (2025) 133554

Contents lists available at ScienceDirect

Separation and Purification Technology

journal homepage: www.elsevier.com/locate/seppur

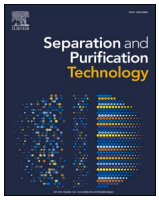

A novel Visbreaking-Supercritical Fluid extraction (SFE) strategy for efficient upgrading of vacuum residue: Experimental optimization and molecular dynamics insights

Shisong Ren [a,*], Ying He [b], Cheng Liu [c], Weiyu Fan [b], Wim Van den bergh [a], Aikaterini Varveri [d]

[a] Sustainable Pavement and Asphalt Research (SuPAR) Group, Faculty of Applied Engineering, University of Antwerp 2020 Antwerp, Belgium
[b] State Key Laboratory of Heavy Oil Processing, China University of Petroleum, Qingdao 266580, China
[c] SINOPEC (Dalian) Research Institute of Petroleum and Petrochemicals Co., Ltd, Dalian 116045, China
[d] Section of Pavement Engineering, Faculty of Civil Engineering & Geosciences, Delft University of Technology, 2628 CN Delft, the Netherlands

ARTICLE INFO

Editor: B. Van der Bruggen

Keywords:
Vacuum Residue
Visbreaking
Supercritical Fluid Extraction
Decarbonization
Demetalization
Molecular Dynamics Simulation

ABSTRACT

The increasing demand for cleaner and more efficient refining processes has driven the development of advanced upgrading technologies for heavy crude residues. This study investigates a novel Visbreaking-Supercritical Fluid Extraction (SFE) approach to upgrade the Merey vacuum residue (VR), integrating experimental analysis with molecular dynamics (MD) simulations for atomic-level mechanism exploration. The Visbreaking process is optimized at 400 °C for 40 min, achieving a viscosity reduction of 89.0 % while minimizing coke formation. The SFE process fractionates the visbroken VR, with total extraction yields ranging from 70.1 wt% to 70.7 wt%, demonstrating remarkable efficiency. Higher extraction pressures enhance deasphalted oil (DAO) yield but compromise its quality with higher metal and sulfur contents, while lower temperatures improve extraction selectivity. The integrated process effectively removes Fe, Ni, V, and Na, with demetalization efficiencies exceeding 62 %, 75 %, and 95 %, respectively. Molecular dynamics simulations provide atomic-scale insights into solubility mechanisms, revealing that higher pressures and lower temperatures enhance solvent compatibility with lighter visbroken VR fractions. The extracted DAO meets marine fuel oil blending specifications, while raffinates show potential for bitumen production and modification. These findings highlight the Visbreaking-SFE combination as a promising and sustainable upgrading strategy for heavy crude residues.

1. Introduction

The global petroleum refining industry faces the dual challenge of processing increasingly heavier crude oils while meeting stricter product quality and environmental regulations. To produce high-quality fuel oils, it is essential to efficiently process heavy crude oils and residues, particularly those with high metal and impurity content. Conventional upgrading technologies for heavy oils include delayed coking, catalytic cracking, and hydrogenation [1]. Visbreaking, as a mild thermal cracking process, offers distinct advantages, including a 20–30 % reduction in capital investment compared to other refining processes, operational efficiency improvements of up to 15–20 %, and a simplified process flow that reduces the number of required units by 30–40 % [2]. Visbreaking reduces the viscosity of residual oils while modifying metal distribution, enabling partial removal of metal contaminants [3]. Compared to catalytic hydroprocessing, which also removes metals but suffers from catalyst deactivation due to metal deposition, Visbreaking provides a cost-effective alternative by eliminating the need for expensive catalysts.

Traditional heavy oil upgrading processes treat the entire feedstock without selectively removing harmful components, leading to lower fuel quality and inefficient resource utilization. To improve conversion efficiency, an effective separation technique is necessary. Supercritical fluid extraction (SFE) has emerged as a promising, environmentally friendly method for selectively separating heavy oil fractions [4]. Conventional separation techniques, such as distillation, solvent extraction, and liquid chromatography, rely on differences in boiling points, solubility, and polarity, respectively, but each has limitations [5]. Distillation struggles with high-boiling fractions due to thermal decomposition risks, while traditional solvent extraction methods have limited

* Corresponding author.
E-mail address: Shisong.Ren@uantwerpen.be (S. Ren).

https://doi.org/10.1016/j.seppur.2025.133554
Received 22 March 2025; Received in revised form 3 May 2025; Accepted 13 May 2025
Available online 14 May 2025

separation capacity and yield fewer distinct fractions.

In contrast, SFE utilizes pressure-dependent variations in solvent density to selectively extract targeted components. This approach offers several advantages, including high yields, superior product quality, minimal thermal degradation, low energy consumption, and strong economic benefits [6]. With fraction yields ranging from 70 % to 95 % by weight, SFE significantly enhances the recovery of valuable lighter fractions [7,8]. It is widely applied in the separation of liquid coke, petroleum residues, and fuel fractions [9–11], as well as in detailed heavy oil characterization due to its high precision [12,13]. Moreover, SFE is gaining attention for its potential in upgrading heavy feedstocks [14–16]. Despite its widespread application, there is limited research on the use of SFE-based hybrid processes in conjunction with other thermal methods, such as Visbreaking, for the demetalization of heavy oils and residues. [17,18].

While optimizing the thermal processing of vacuum residue is crucial for enhancing deasphalted oil (DAO) yield and purifying chemical components through decarbonization and demetalization, the fundamental interaction mechanisms between vacuum residue components and solvents remain poorly understood [19]. Molecular dynamics (MD) simulations provide a powerful computational framework for unravelling these complex molecular interactions during Visbreaking and supercritical fluid extraction [20]. MD simulations allow for a detailed investigation of the thermodynamic and kinetic behaviors of heavy hydrocarbons in the presence of supercritical solvents, offering insights into key mechanisms such as molecular diffusion [21], solvent penetration [22], and asphaltene aggregation [23]. By offering atomic-scale insights, MD simulations aid in optimizing reaction conditions, improving solvent selection, and enhancing overall process efficiency [24]. However, the challenge lies in defining, studying, and measuring these molecular interactions experimentally, which complicates the development of more effective upgrading strategies for heavy crude residues.

This study investigates a combined Visbreaking-supercritical fluid extraction (SFE) process for the removal of metals from vacuum residue. The feedstock used is the Merey vacuum residue, an ultra-heavy oil characterized by high viscosity, elevated metal content, and significant asphaltene concentration, making it particularly difficult to process [25]. The integration of Visbreaking with SFE offers several advantages over standalone SFE. First, the Visbreaking step reduces the viscosity of the feedstock, facilitating its transport into the extraction column and enhancing mass transfer efficiency, which improves the yield of extracted fractions compared to SFE alone. Additionally, metals and high-carbon components predominantly accumulate in asphaltenes and coke rather than in the extracted fractions, reducing their contamination in the final product. Compared to conventional solvent deasphalting (SDA), SFE provides lower energy consumption and more efficient solvent recycling [26,27]. Furthermore, this integrated approach is expected to yield higher quantities of light oil and provide improved economic benefits. Therefore, the research will address the following questions: (i) How does the integrated approach enhance light oil production compared to traditional methods? (ii) How the key factors affect the Visbreaking-SFE products? (iii) What are the molecular-scale interaction mechanisms driving the high extraction efficiency during the SFE process?

2. Research objective and methodology

To enhance the utilization efficiency of vacuum residue, this study aims to introduce a novel approach for decarbonization and demetalization through a Visbreaking-supercritical fluid extraction (SFE) combination process. Meanwhile, the atomic-level understanding of the interaction mechanisms between solvent and vacuum residue molecules will provide valuable insights for optimizing SFE process conditions and selecting highly efficient solvents. The research methodology in this study shown in Fig. 1 integrates experimental and computational approaches to investigate the Visbreaking-supercritical fluid extraction process for upgrading vacuum residue. The experimental section consists of thermal Visbreaking and SFE applied to the Merey VR using n-pentane as the solvent. Visbreaking experiments are conducted at variable temperatures and reaction times, while SFE is performed at different pressures and temperatures condition. Key product characteristics, such as density, viscosity, Conradson carbon residue, sulfur content, and metal composition, are analysed to assess process efficiency. In

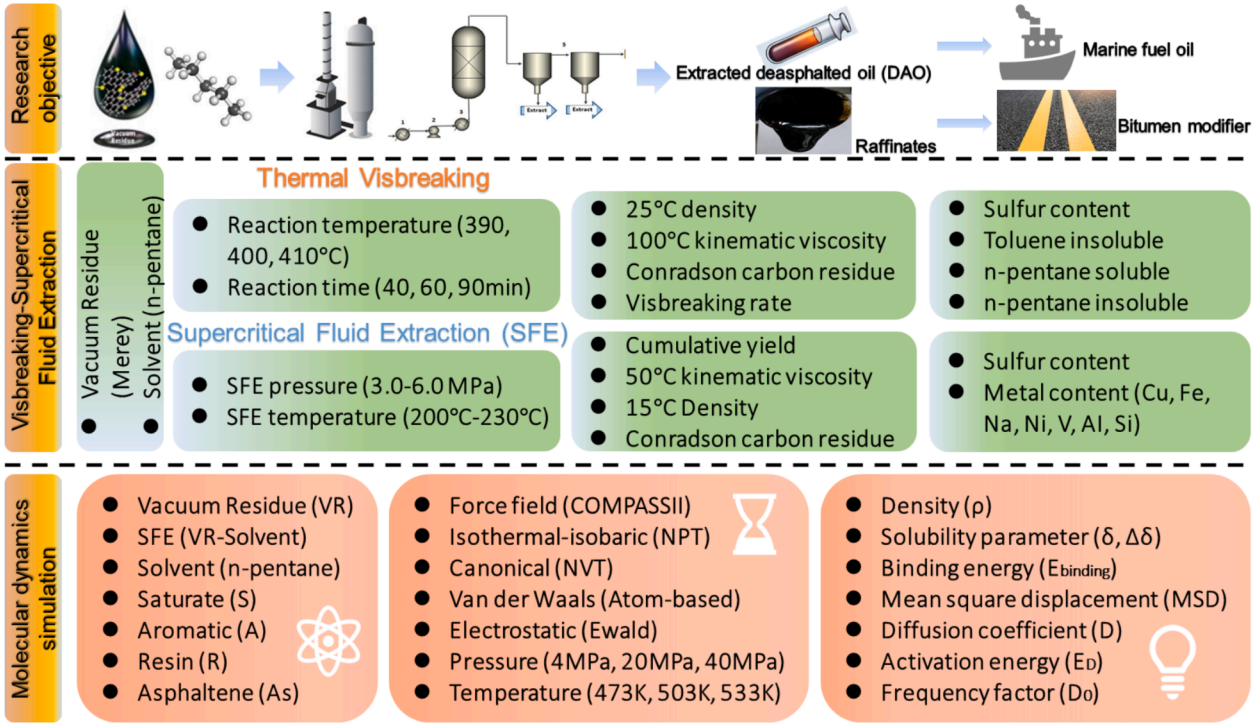

Fig. 1. Research objective and methodology.

parallel, molecular dynamics (MD) simulations are employed to gain fundamental insights into the molecular interactions between visbroken VR components and the solvent. The thermodynamic and kinetic behavior of the system at different pressures and temperatures are elucidated through the key properties of density, solubility parameters, binding energy, mean square displacement, and diffusion coefficient. This comprehensive approach enables a deeper understanding of the Visbreaking-SFE process and provides critical insights into optimizing vacuum residue upgrading for industrial applications.

3. Materials and methods

3.1. Raw materials

The feedstock used in this study is vacuum residue (VR) derived from Venezuela Merey heavy crude oil, with its key properties summarized in Table 1. The solvent selected for supercritical fluid extraction (SFE) is commercially pure n-pentane, with a purity exceeding 98 %, as verified by gas chromatography. The fundamental properties of n-pentane are provided in Table 2. Experimental analysis reveals that Merey VR is of low quality, characterized by high density, high viscosity, elevated sulfur content, and significant metal concentrations, particularly sodium (Na) and vanadium (V). Furthermore, the high asphaltene content in Merey VR suggests a high propensity for coking reactions during thermal cracking, posing challenges for upgrading and refining processes. The n-pentane is chosen as the supercritical solvent due to its superior solvency for heavy hydrocarbon fractions compared to supercritical carbon dioxide (Sc-CO_2). While Sc-CO_2 offers advantages in energy efficiency and safety, its lower solubility parameter and significant density drop at high temperatures limit its effectiveness for extracting polarizable and aromatic-rich components from visbroken vacuum residue. The critical temperature, critical pressure, and critical density of n-pentane is reported as 196.4 °C, 3.37 MPa, and 0.232 g/cm^3. These values are essential reference points for defining the supercritical region of n-pentane, beyond which it exhibits unique solvent power with enhanced diffusivity. In this study, all SFE experiments are conducted at pressures and temperatures exceeding these critical thresholds to ensure operation within the supercritical regime.

3.2. Visbreaking procedure

All Visbreaking experiments are conducted using a high-pressure reactor equipped with a 500 mL stainless steel vessel. A 250 mL sample of Merey VR is introduced into the reactor. To ensure proper sealing, a pressure test is performed using nitrogen injection, followed by purging to eliminate any residue air. The system is then pressurized to a constant 2.0 MPa before initiating the reaction. This pressure is selected to reflect typical industrial visbreaking conditions and to maintain operational safety and reproductivity in the laboratory setting. The reaction temperature is varied between 390 °C and 410 °C, which represents a moderate thermal severity commonly used to minimize coke formation while enabling effective cracking of heavy components in vacuum residue [2]. The batch time ranges from 40 to 90 min. Upon completion of the reaction, the reactor is immediately quenched using cooling water to halt further thermal cracking. Once the temperature returns to ambient conditions, the visbroken products are collected and the visbreaking rate at different thermal conditions are calculated as **Eq.1**. In addition, the physical and chemical properties of visbroken products are measured, including density, kinematic viscosity, sulfur content and Conradson Carbon Residue (CCR) content.

$$Visbreakingrate(\%) = \left(\frac{W_{feed} - W_{residue}}{W_{feed}}\right) \times 100 \quad (1)$$

where W_{feed} and $W_{residue}$ are the weight of vacuum residue feedstock and unconverted residue after visbreaking (g), respectively.

Table 1
Physical and chemical properties of Merey vacuum residue.

Properties	Measured value	Test Standard
Density at 20 °C (kg·m^{-3})	1025.5	ASTM D1480 [28]
Kinematic viscosity at 100 °C (mm^2·s^{-1})	2734	ASTM D445 [29]
Sulfur content (wt %)	3.77	ASTM D7679 [30]
CCR (wt %)	19.23	ASTM D189 [31]
Toluene insoluble (wt%)	0.012	ASTM D4072 [32]
n-pentane soluble (wt%)	68.4	ASTM D4055 [33]
n-pentane insoluble (wt%)	31.6	
Vitriol (V, mg·kg^{-1})	234.4	STP11992S [34]
Nickel (Ni, mg·kg^{-1})	54.5	
Sodium (Na, mg·kg^{-1})	109.8	
Aluminium + Silicon (Al + Si, mg·kg^{-1})	15.22	

Table 2
Chemical and physical properties of n-pentane solvent.

Items	Result	Items	Result
Chemical formula	C_5H_{12}	Boiling point (°C)	36.1
Molecular weight	72.15	Critical temperature (°C)	196.4
Appearance	Colourless liquid	Critical pressure (MPa)	3.37
n-pentane mass percentage (wt%)	99.169	Critical density (g/cm^3)	0.232

3.3. Supercritical fluid extraction and fractionation process

Fig. 2 presents schematic diagram of the supercritical fluid extraction and fractionation (SFEF) apparatus. In the extraction process, the feedstock is introduced from the top of the extraction column, while the solvent (n-pentane) is fed from the bottom. Within the extractor, the vacuum residue (VR) dissolves into the supercritical pentane, and a packed bed in the filling section ensures intimate contact between the feedstock and the solvent, facilitating efficient extraction. A temperature gradient is maintained across the SFEF apparatus, with the top temperature consistently higher than the bottom temperature. The extraction process is regulated by adjusting the extraction pressure, ensuring optimal separation of fractions. Upon completion of the supercritical extraction, the deasphalted oil (DAO) fractions and raffinates are collected for further property analysis. The operating conditions of the SFE process are as follows [35]: (i) Solvent flow rate: 90 mL/min; (ii) Temperature gradient (top > bottom of extractor): 10 °C; (iii) Pressure rise rate: 0.067 MPa/min; (iv) Feedstock quantity: 1000 g. Various SFE pressures and temperatures are adopted to evaluate their effects on extraction efficiency and deasphalted oil (DAO) quality, as summarized in Table 3. Each marked point in this table represents a separate SFE run conducted under one specific pressure and temperature condition. This experimental design allows for the evaluation of the individual and combined effects of pressure and temperature on the SFE extraction process. The visbroken products and fractions obtained from extraction are characterized based on the specifications outlined in Table 1. To ensure accuracy and minimize deviations, each sample is measured three times.

4. Experimental results and discussion

4.1. Evaluation on visbroken products

The Visbreaking process of Merey VR is conducted to evaluate the effects of reaction temperature and reaction time on visbroken product properties. The results, presented in Table 4 and 5, indicate that the density of visbroken products decreases slightly with increasing temperature and prolonged reaction time. However, the sulfur content and Conradson carbon residue (CCR) remain relatively unchanged across

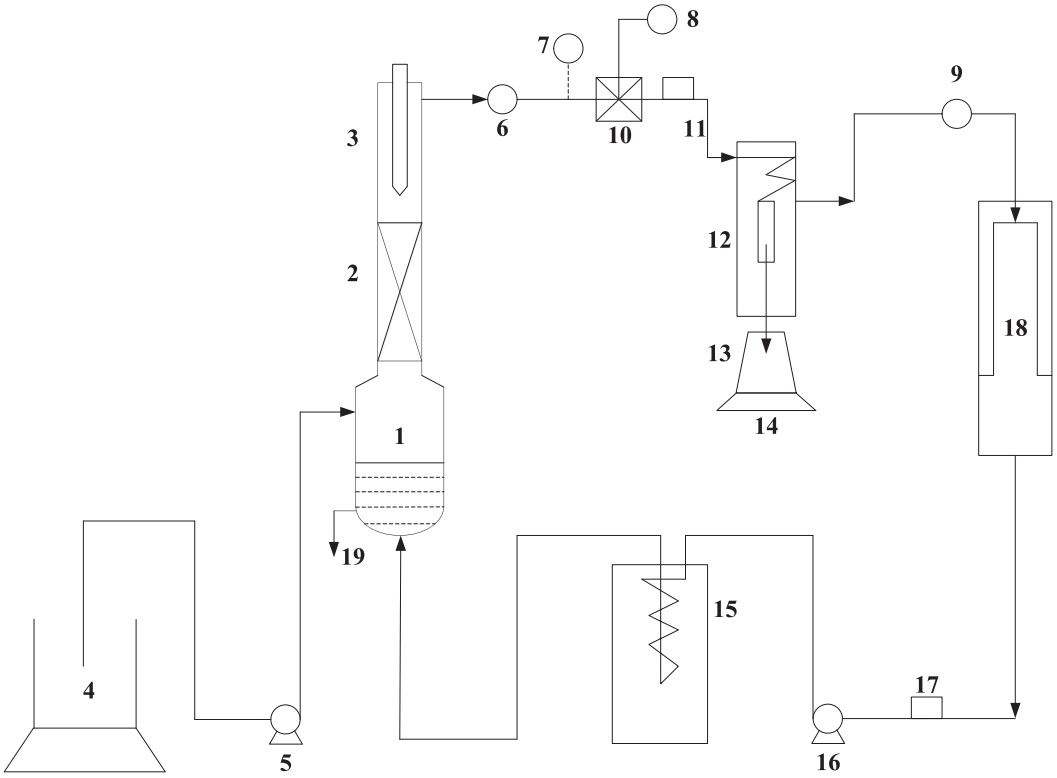

Fig. 2. Schematic diagram of SFE apparatus. (1) extraction section, (2) filling section, (3) electrothermal reflux heater, (4) raw material bucket, (5) raw material pump, (6), (9) condenser, (7) pressure gage, (8) pressure control system, (10) pressure-regulating valve, (11) observation window, (12) fractional condenser, (13) sampling bottle, (14) electronic balance, (15) solvent preheating furnace, (16) solvent pump, (17) filter, (18) solvent furnace, (19) discharge chute.

Table 3
Supercritical Fluid Extraction (SFE) temperatures and pressures used in this study.

P T	3.0 MPa	3.5 MPa	4.0 MPa	4.5 MPa	5.0 MPa	5.5 MPa	6.0 MPa
200 °C	●	●	●	●			
205 °C	●	●	●	●	●		
210 °C	●	●	●	●	●	●	
220 °C	●	●	●	●	●	●	●
230 °C			●	●	●	●	●

Table 4
Visbreaking conditions and properties of visbroken Merey VR.

No.	Reaction temperature (°C)	Reaction time (min)	20 °C Density ($kg \cdot m^{-3}$)	100 °C Kinematic viscosity ($mm^2 \cdot s^{-1}$)	Sulfur content (wt %)	CCR (wt %)
1	390	40	1021.3	460.5	1.07	14.77
2	390	60	1018.0	347.0	1.23	14.56
3	390	90	1015.3	205.7	1.24	14.48
4	400	40	1012.2	301.6	1.26	14.32
5	400	60	1010.6	187.2	1.33	14.28
6	400	90	1009.2	162.9	1.27	14.23
7	410	40	1007.4	190.4	1.29	13.95
8	410	60	1005.8	157.6	1.24	13.91
9	410	90	1004.1	152.3	1.20	13.84

different reaction conditions. To assess coking tendency, toluene insoluble (TI), n-pentane soluble (NPS), and n-pentane insoluble (NPI) fractions are used as key indicators. As shown in Table 4, higher reaction temperatures and extended reaction times result in a gradual decrease in n-pentane soluble and a corresponding increase in n-pentane insoluble, indicating coke formation [36]. At 400 °C for 40 min, the toluene insoluble fraction of visbroken Merey VR is 0.012 wt%, closely matching that of the original Merey VR, suggesting minimal coke formation under these conditions. However, when the reaction time is further extended at 400 °C, or when the temperature is increased to 410 °C for 40, 60, and 90 min, severe coking occurs, indicating that these conditions exceed the thermal stability limit of the feedstock.

The correlation curves between reaction time and the physical properties of visbroken products, including density, kinematic viscosity, sulfur content, and Conradson carbon residue CCR, are presented in Fig. 3 to explore the visbreaking kinetics of vacuum residue. As reaction time increases, most physical properties (density, viscosity, CCR) exhibit an exponential decline. However, their rates of decrease vary significantly depending on reaction temperature. In contrast, sulfur content initially decreases sharply but stabilizes at approximately 1.25 wt% beyond 40 min of reaction time, likely due to the limited formation of sulfur-containing gases during the thermal visbreaking process [37]. Correlation equations indicate that higher temperatures accelerate the reduction rates of density, viscosity, and CCR in visbroken products as a function of reaction time, demonstrating that elevated temperatures enhance visbreaking efficiency for vacuum residue. Notably, the rate of CCR reduction exceeds that of kinematic viscosity, followed by density, suggesting that thermal visbreaking is more effective at lowering CCR and viscosity than density. Furthermore, when the reaction time extends beyond 60 min, the reduction of all these physical properties reaches a plateau, even at high temperatures, indicating a diminishing effect of prolonged Visbreaking. Lastly, it is important to note that the physical properties of visbroken products at different reaction times and

Table 5
Visbreaking conditions and the evaluation of coking tendency.

No	Reaction temperature (°C)	Reaction time (min)	Toluene insoluble (wt %)	n-pentane soluble (wt%)	n-pentane insoluble (wt%)	Visbreaking rate (%)
1	390	40	0.016	81.59	18.41	83.2
2	390	60	0.042	79.68	20.32	87.3
3	390	90	0.091	78.99	21.01	92.5
4	400	40	0.042	80.03	19.97	89.0
5	400	60	1.047	77.13	22.87	93.2
6	400	90	4.492	74.49	25.51	94.0
7	410	40	1.066	76.10	23.90	93.0
8	410	60	6.245	69.11	30.89	94.2
9	410	90	11.62	66.46	33.54	94.4

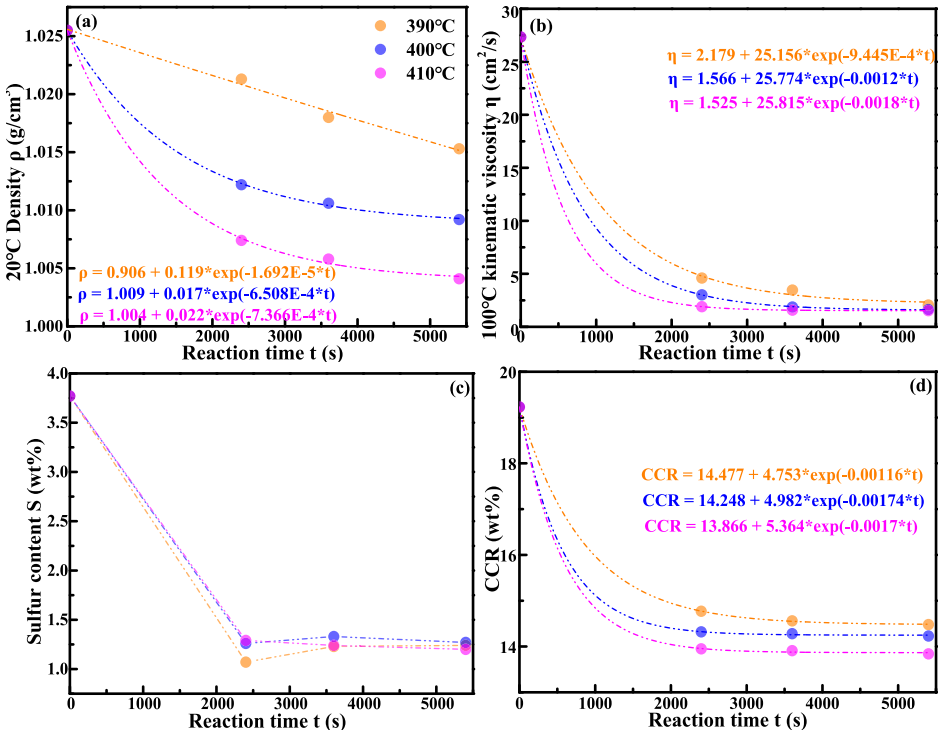

Fig. 3. The correlations between the density, viscosity, sulfur content, and CCR with reaction time.

temperatures can be accurately predicted using kinetic correlation models.

At a constant reaction temperature, kinematic viscosity decreases, and the Visbreaking rate increases with prolonged reaction time. Similarly, at a fixed reaction time, increasing the reaction temperature leads to a further reduction in viscosity. These findings indicate that higher temperatures and longer reaction times accelerate the thermal cracking reaction, enhancing the viscosity reduction effect. As shown in Table 5, at 400 °C, the Visbreaking rate improves with an extended reaction time of 90 min, but the improvement is marginal compared to 40 min and 60 min. Additionally, longer reaction times result in higher energy consumption and an increase in toluene-insoluble content, signalling the onset of coke formation. The objective of the Visbreaking process is to lower the viscosity of Merey VR while preventing excessive coke formation. A comprehensive analysis suggests that mild thermal cracking conditions yield higher-quality visbroken products with improved utilization efficiency before thermodynamic limitations. The results show that Sample No.4 exhibits no coke formation during the Visbreaking process and achieved a high Visbreaking rate of 89.0 %. This indicates that the optimal conditions for deep thermal cracking of Merey VR without coke formation are 400 °C for 40 min, achieving a maximum visbreaking rate of approximately 89.0 %. It is important to note that the feedstock used for the Supercritical Fluid Extraction (SFE) process is visbroken Merey VR obtained under the optimized thermal visbreaking conditions of 400 °C, 2.0 MPa, and 40 min.

Fig. 4 illustrates the variation trends of Toluene insoluble (TI), n-pentane insoluble (NPI), n-pentane soluble (NPS), and Visbreaking rate (VR) in visbroken products as a function of reaction time. As reaction time increases, TI, NPI, and VR exhibit an exponential rise, while NPS follows an exponential decline. Higher Visbreaking temperatures lead to a pronounced increase in TI, NPI, and VR, accompanied by a corresponding decrease in NPS. Similar to the trends observed in physical properties, the rate of change in these chemical properties and the Visbreaking rate strongly depend on reaction temperature. Specifically, as the reaction temperature increases from 390 °C to 410 °C, the growth rates of TI and NPI accelerate, while the decline rate of NPS reaches its peak at 410 °C. Additionally, at elevated temperatures, the Visbreaking rate increases at a slower rate, suggesting that higher reaction temperatures enhance the overall Visbreaking efficiency but reduce its sensitivity to reaction time. These findings highlight the critical role of temperature in optimizing Visbreaking performance and controlling the chemical composition of the final visbroken products.

4.2. *Evaluation on DAO fractions*

The Supercritical Fluid Extraction (SFE) process of visbroken Merey

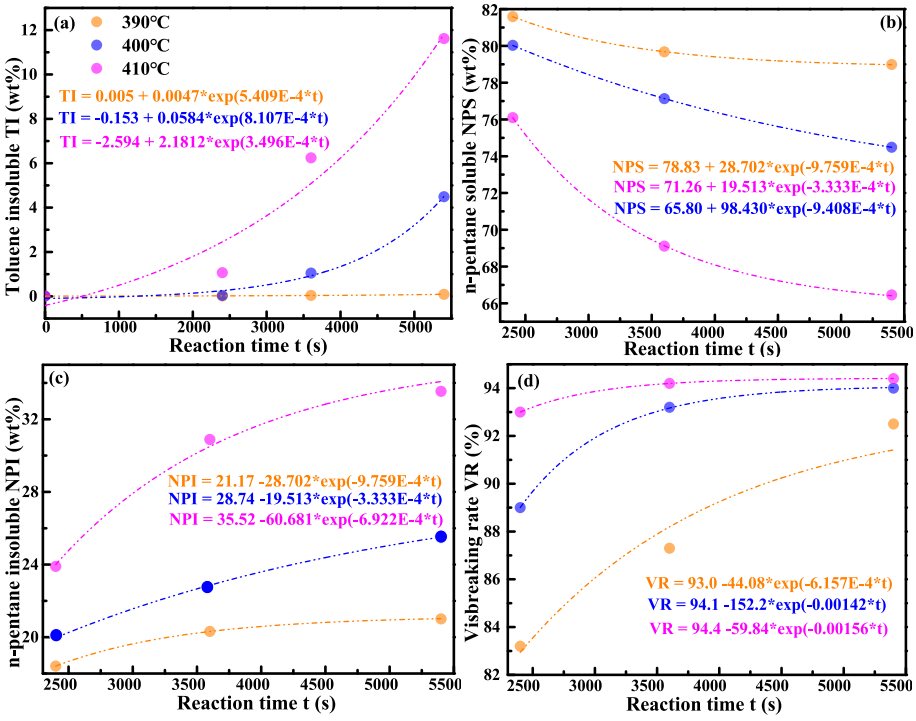

Fig. 4. The correlations between the TI, NPS, NPI, and VR values with the reaction time.

VR is conducted to evaluate the effects of reaction temperature and pressure on extraction efficiency. The results, presented in Fig. 5, Fig. 6, and Fig. 7, provide insights into the influence of these parameters on the separation performance. In this study, visbroken Merey VR product No.7 is selected as the feedstock for the SFE process. The cumulative yield of deasphalted oil (DAO) from the SFE process of vacuum residue is calculated using **Eq.2**.

$$Cummulativeyield(wt\%) = \left(\frac{W_{DAO}}{W_{feed}}\right) \times 100 \quad (2)$$

where W_{feed} and W_{DAO} are the initial mass of vacuum residue feed to SFE process and total mass of deasphalted oil (g), respectively.

As illustrated in Fig. 5, the cumulative deasphalted oil (DAO) yield exceeds 70 wt%, demonstrating the efficiency of the extraction process. At a constant temperature, the DAO yield increases with rising pressure, particularly at lower pressures where a rapid increase is observed. However, once the pressure reaches a certain threshold, the yield growth slows, and further pressure increase has minimal impact. Additionally, at a fixed DAO yield, achieving higher extraction temperatures requires higher operating pressures. Conversely, at a constant pressure, the DAO yield increases as the temperature decreases. These findings suggest that n-pentane exhibits enhanced dissolving capacity when the temperature is lowered and pressure is increased to an optimal level, leading to an improved DAO yield.

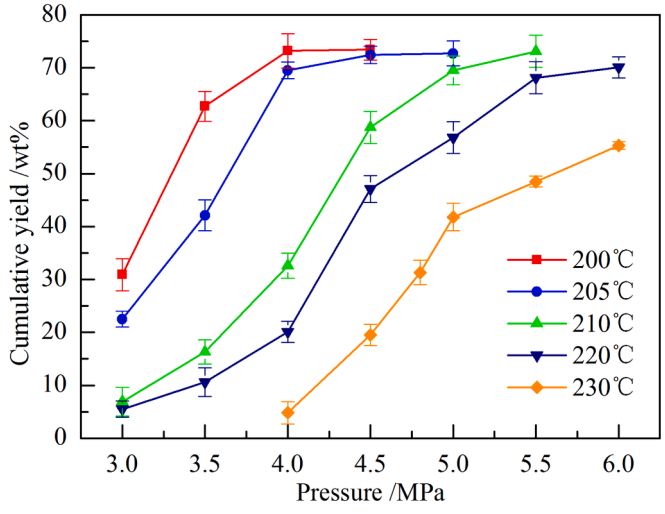

Fig. 5. Supercritical extraction yields of the visbroken Merey VR under different temperatures.

The exponential relationship between the cumulative yield (CY) and pressure (P) are observed and described using **Eq.3** to quantitatively explore the effect of SFE pressure on the DAO yield.

$$CY = a*\exp(k*P) + b \quad (3)$$

where a is a scaling factor that determines the initial magnitude of the exponential term, and k denotes the exponential growth (or delay) rate and dictates the sensitivity of CY to changes in P. Moreover, b is a constant offset that shifts the entire function up or down, representing a baseline value of CY when P = 0.

The correlation curves and equations of CY as a function of pressure (P) for DAO at different supercritical fluid extraction (SFE) temperatures are presented in Fig. 6**(a)**. The results indicate that SFE temperature has a negative impact on DAO yield, whereas pressure exerts a positive influence. Furthermore, temperature significantly affects the pressure sensitivity of DAO yield, as evidenced by the gradual decline in the CY index's rate of increase with pressure at higher temperatures. This suggests that elevated temperatures not only reduce DAO yield but also weaken the positive effect of pressure on cumulative DAO yield. To describe the SFE temperature effect on the pressure sensitivity parameter (k) in a convenient mathematical form, one empirical equation (shown below) is employed.

$$Lnk = \frac{E_a}{R} \bullet \frac{1}{T} + Ln(A) \quad (4)$$

where E_a represents the activation energy (J/mol), R is the universal gas constant (8.314 J/mol·K^{-1}), and A is the pre-exponential factor. The In

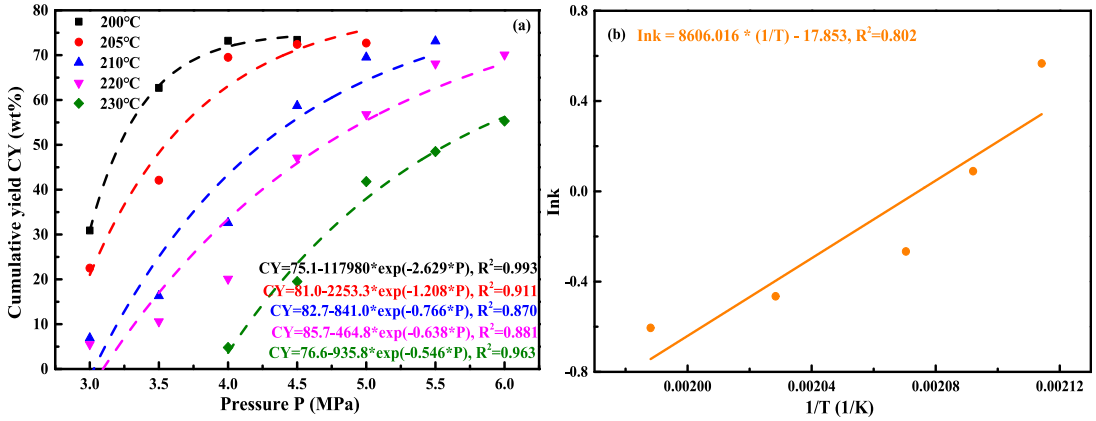

Fig. 6. The correlation curves of cumulative yield-pressure and Ink-1/T.

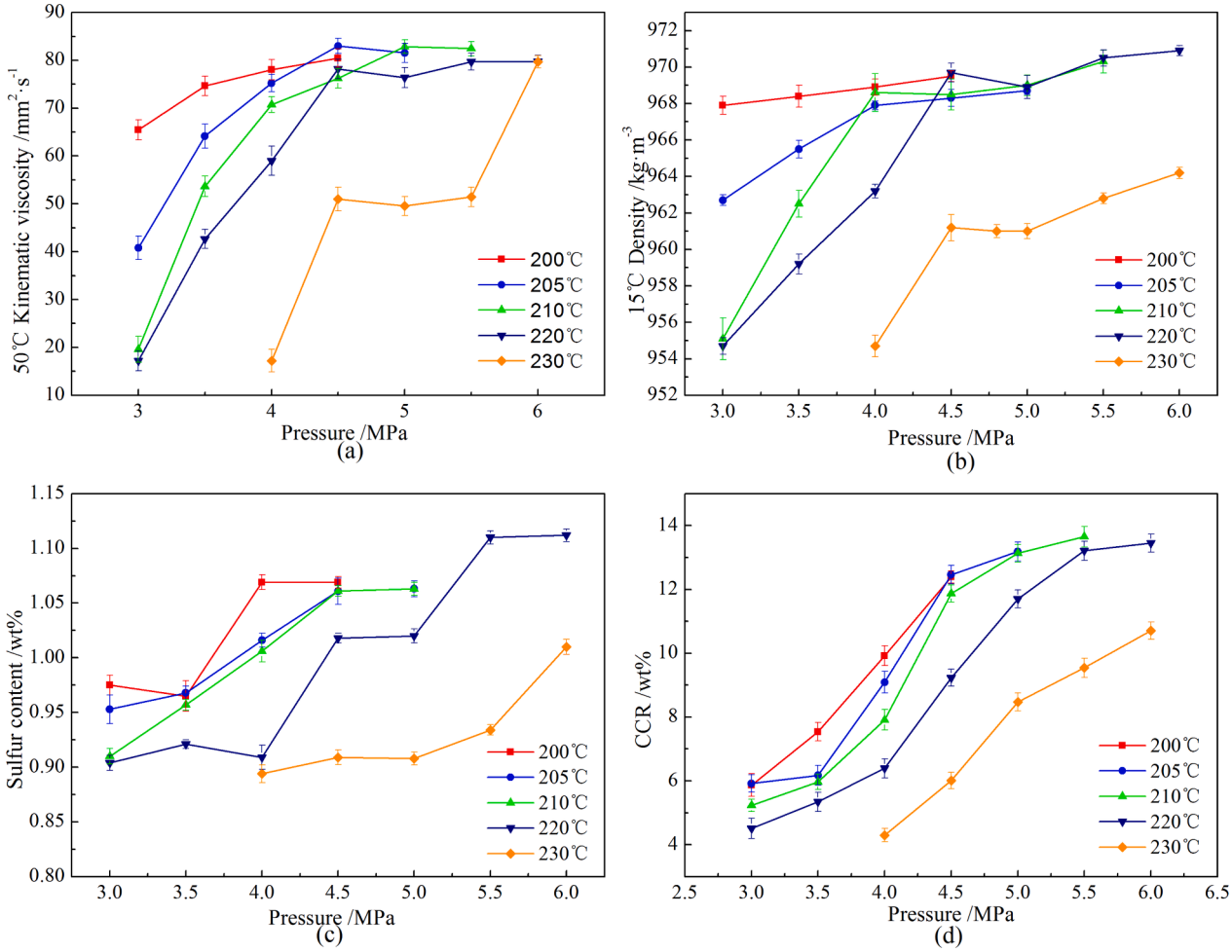

Fig. 7. Properties of SFEF narrow fractions under different extraction conditions. (a) Kinematic viscosity, (b) Density, (c) Sulfur content and (d) CCR content.

(k) versus 1/T curve is plotted in Fig. 6**(b)**, showing a linear increase in Ink with increasing 1/T. Furthermore, the calculated values of E_a and A in this study are 71550.4 J/mol AND 1.764E-8, respectively. Using the established correlation equation, the k values at different temperatures can be accurately predicted.

The properties of Supercritical Fluid Extracted Fractions (SFEF) under varying extraction conditions are presented in Fig. 7. The results indicate that at a constant temperature, kinematic viscosity, density, sulfur content, and Conradson Carbon Residue (CCR) increase with rising extraction pressure. The observed trends can be categorized into two distinct phases based on the yield growth rate: a rapid growth period followed by a steady growth period. Furthermore, it is observed that higher extraction temperatures necessitate greater pressures to transition from the rapid growth phase to the steady phase. This suggests that temperature and pressure are interdependent factors in controlling the composition and properties of the extracted fractions, emphasizing the need for optimized extraction conditions to achieve the desired product characteristics.

The metal content in Supercritical Fluid Extracted Fractions (SFEF) extracted from visbroken vacuum residue is illustrated in Fig. 8. It indicates that metal concentration in extracted fractions increases with rising extraction yield, following the order: Cu < (Al + Si) < Na < Fe < Ni < V. This is due to the increased extraction of heavier fractions containing metal elements in the DAO phase. Notably, the vanadium (V) content remains below 65 $mg{\cdot}kg^{-1}$, while other metals are below 15 $mg{\cdot}kg^{-1}$ in the deasphalted oil (DAO). The concentrations of V and Na in DAO are reduced by an order of magnitude compared to the original Merey VR, demonstrating the strong demetalization efficiency of the Visbreaking-SFE process. Additionally, the extracted DAO fractions exhibit significantly lower density, viscosity, Conradson Carbon Residue (CCR), sulfur, and metal content than the feedstock. These findings confirm that the Visbreaking-SFE combination process produces higher-quality products compared to conventional Visbreaking alone, making it a more effective upgrading strategy for heavy crude residues.

4.3. Evaluation on decarbonization and demetalization

To compare the single Supercritical Fluid Extraction (SFE) process with the Visbreaking-SFE combination process, SFE is conducted separately on both Merey VR and visbroken Merey VR under identical operating conditions. In this study, the bottom and top temperatures of the extraction column are set at 220°C and 230 °C, respectively, while the increase rate of initial pressure, terminal pressure, and pressure remain consistent for both feedstocks. During the SFE process, seven narrow fractions and the raffinates are collected and analysed. The results show that the total liquid yield extracted from Merey VR is 68.4 wt %, with raffinate yield at 31.6 wt%, whereas for visbroken Merey VR, the total liquid yield increases to 70.1 wt%, and raffinate yield decreases to 29.9 wt%. These findings indicate that the SFE process achieves better decarbonization efficiency when applied to visbroken Merey VR compared to untreated Merey VR. The improved decarbonization effect of the Visbreaking-SFE combination process can be attributed to the thermal cracking reactions during Visbreaking, while facilitate the conversion of heavy components into extractable fractions [38]. As demonstrated in this study, visbroken Merey VR contains a higher proportion of heavy components that cannot be extracted by n-pentane, suggesting that condensation reactions occurring during Visbreaking enhance the efficiency of the subsequent SFE process.

As shown in Fig. 9, under identical extraction conditions and at the same cumulative yield, the metal content in extracted fractions from visbroken Merey VR is significantly lower than that from untreated Merey VR. This demonstrates the strong demetalization efficiency of the Visbreaking-SFE combination process. A comparison between Merey VR and its corresponding deasphalted oil (DAO) fractions reveals that the demetalization rates for Fe, Ni, V, and Na exceed 62 wt%, 75 wt%, and 95 wt%, respectively. Furthermore, when comparing the single SFE process with the Visbreaking-SFE combination process, it is evident that the mild thermal cracking in Visbreaking enhances the yield of light components, while condensation reactions contribute to a reduction in metal content within the DAO fractions. The DAO products derived from the Visbreaking-SFE process exhibit high quality, optimized product distribution, and increased target product yield. Notably, only trace amounts of metals and impurities are extracted from visbroken Merey VR, making the DAO fractions highly suitable as blending components for marine fuel oils, which impose strict limits on metal content.

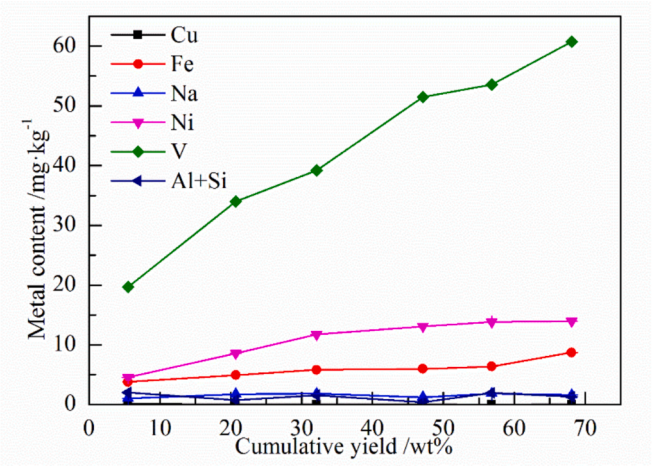

Fig. 8. Metal content in SFE narrow fractions extracted from visbroken vacuum residue.

According to the latest marine fuel specifications outlined in ISO 8217:2017 [39], specific limits are imposed on the concentrations of vanadium (V), sodium (Na), and aluminium + silicon (AI + Si). The metal content requirements for various grades of residue marine fuels are summarized in Table 6, highlighting the differing metal limits across fuel types. As shown in Fig. 9, when the cumulative DAO yield is below 32.1 wt%, the V content is less than 50 mg/kg. Additionally, across all cumulative yield levels examined in this study, the Na and AI + Si contents in DAO meet the marine fuel requirements. Based on these findings, the DAO fractions obtained in this work demonstrate sufficient low metal content, making them a suitable blending component for marine fuel oils.

Related research has demonstrated that raffinates can be effectively utilized as blending components for bitumen production, particularly in the formulation of hard bitumen [40]. Additionally, they can serve as bitumen modifiers, anti-rutting agents, and potential substitutes for lake bitumen, enhancing the performance and durability of bituminous materials. Furthermore, the results of this study confirm that the Visbreaking-SFE combination process is highly suitable for processing low-quality residues with high metal content and elevated asphaltene concentrations. This integrated approach not only offers significant economic benefits but also aligns with stringent environmental regulations, reinforcing its potential for widespread industrial application.

5. Molecular dynamics (MD) simulations

Based on the experimental results, it is observed that supercritical extraction conditions, specifically temperature and pressure, have a significant impact on the cumulative yield, physical properties (kinematic viscosity and density), and chemical composition (sulfur content, Conradson carbon residue (CCR), and metal content) of the DAO fraction. Notably, no chemical reaction occurs among vacuum residue components during the SFE process. However, atomic-scale thermodynamic and solubility interactions between visbroken vacuum residue components and the solvent under varying temperature and pressure conditions play a crucial role in determining SFE efficiency and the distribution of components between the DAO and raffinate fractions. These factors, in turn, influence the quality of marine fuels and bituminous materials. Hence, a fundamental understanding of the molecular interactions and solubility mechanisms governing the SFE process is essential. To achieve this, molecular dynamics (MD) simulations are employed to elucidate and predict solubility behavior of visbroken vacuum residue and solvent molecules under different temperature and pressure conditions during the SFE process.

5.1. Molecular models of SARA fractions in visbroken vacuum residue

The chemical composition of visbroken vacuum residue is categorized into distinct groups based on molecular weight and polarity, namely saturate (S), aromatic (A), resin (R), and asphaltene (As). Using thin-layer chromatography with flame ionization detection (TLC-FID), the SARA fractions of visbroken Merey vacuum residue obtained under the optimized thermal visbreaking conditions of 400 °C, 2.0 MPa, and 40 min were determined as follows: 14.44 wt% saturate, 46.28 wt%

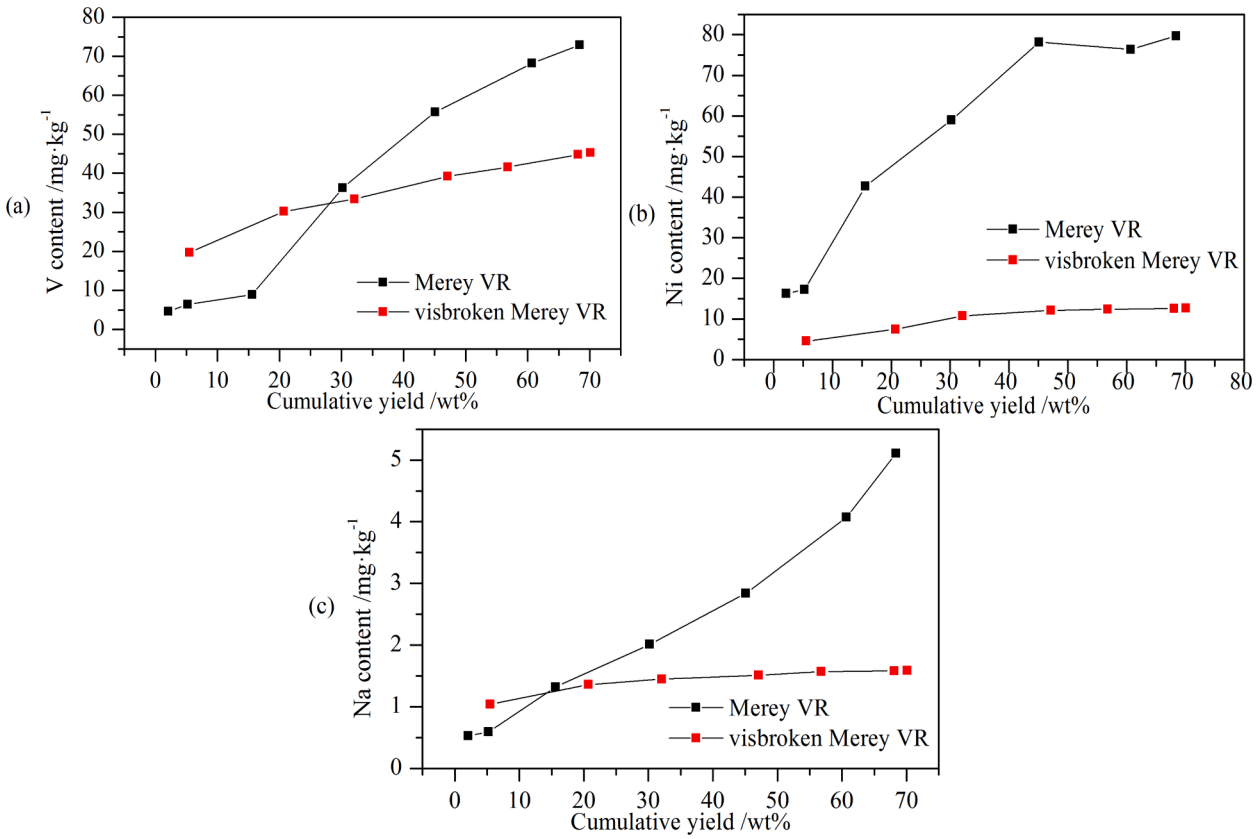

Fig. 9. Metal content in SFEF fractions extracted from VR and visbroken VR. (a) V, (b) Ni, (c) Na content.

Table 6
Residual marine fuels [39].

Characteristics	Unit	Limit	Category ISO-F-			
			RMD80	RME180	RMG180	RMG380
V	mg/kg	Max	150	150	350	350
Na	mg/kg	Max	100	50	100	100
Al + Si	mg/kg	Max	40	50	60	60

aromatic, 26.08 wt% resin, and 13.20 wt% asphaltene. To construct a molecular model of the visbroken vacuum residue, the 12-component model for SARA fractions proposed by Li and Greenfield was adopted as the foundation, as illustrated in Fig. 10 [41].

This model has been reported to successfully predict the thermodynamic behavior of heavy oils and bituminous materials based on their elemental composition, functional group distribution, and molecular size. Furthermore, molecular structures of the SARA fractions were developed for different levels of oxidative aging [42]. To distinguish

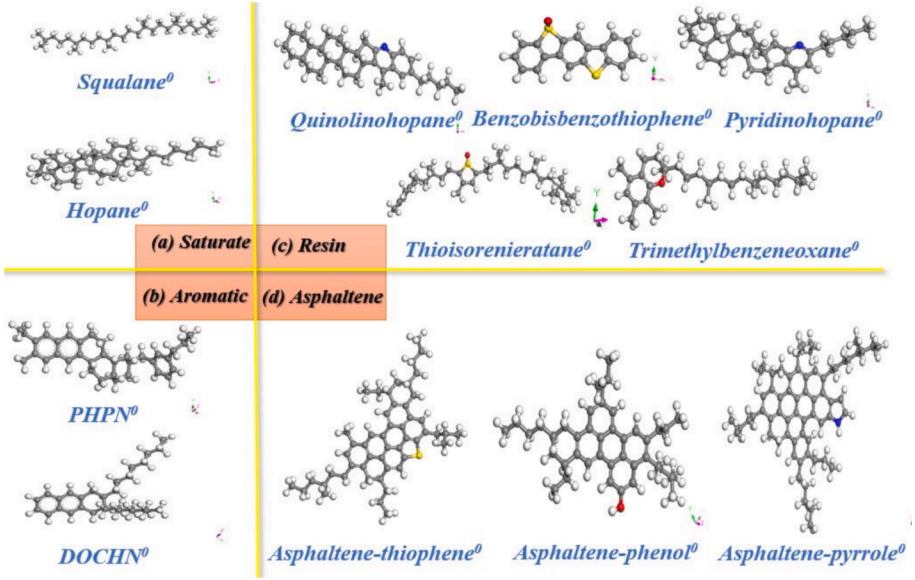

Fig. 10. The molecular structures of SARA fractions in visbroken vacuum residue [41].

between fresh and aged structures, the superscript "0″ is assigned to the fresh components. Based on the experimental SARA results, the molecular quantities and chemical formulas of the various SARA components in visbroken vacuum residue are determined and presented in Table 7. The SARA fractions in the molecular model closely align with the experimentally measured values, with minor discrepancies attributed to the rounding of molecular numbers to whole integers.

5.2. MD simulation procedure and validation

To construct the SFE model, n-pentane solvent molecules are randomly introduced into the visbroken vacuum residue model. During the SFE process, the solvent is injected at a rate of 90 mL/min with a density of 0.629 g/cm^3, resulting in a mass injection rate of approximately 56.61 g/min. Given that the total mass of visbroken vacuum residue (visbroken VR) is 1000 g, the solvent accounts for 5.36wt% per minute. Consequently, the number of solvent molecules involved into the solvent-visbroken VR model per minute is determined to be 30. Additionally, molecular models for the solvent (n-pentane), saturate, aromatic, resin, and asphaltene are developed to evaluate their solubility parameters and investigate their compatibility with the solvent in the SFE process.

The molecular distributions of the solvent and SARA fraction models are summarized in Table 8. It is important to ensure that the molecular ratio of different components within the SARA models remains consistent with that in the visbroken VR model to maintain an accurate representation of the system. For all models, the molecular dynamics (MD) simulation process for initializing the system consists of two key stages: energy minimization and pre-equilibration. Initially, geometry optimization is performed for each molecule to identify the most stable configuration with minimal energy. Following this, molecular models of visbroken VR, solvent-visbroken VR, solvent, and SARA fractions are constructed using the COMPASSII force field. This force filed is widely recognized for accurately representing the molecular interactions of heavy oil and is particularly effective in predicting the thermodynamic properties of bituminous materials. The detailed interaction terms governing the COMPASSII force field can be found in previous studies [42,43]. To generate the initial models, all molecules are randomly placed within a cubic simulation box at an initial density of 0.1 g/cm^3. Subsequently, energy minimization is applied to eliminate atomic overlaps and stabilize the system.

After initialization, molecular dynamics simulations are carried out to achieve pre-equilibrated molecular models. These simulations are conducted under both the isothermal-isobaric (NPT) and canonical (NVT) ensembles for 200 picoseconds (ps), with a time step of 1 fs (fs). The Andersen barostat and Nose thermostat are employed to regulate pressure and temperature conditions. Different MD simulations on all models will run at different temperatures (473 K, 503 K, and 533 K) and pressures (4 MPa, 20 MPa, and 40 MPa). For non-bonded molecular interactions, both Van der Waals and electrostatic forces are considered. The calculations of these interactions are performed using an atom-based approach with a cut-off distance of 12.5Å for Van der Waals forces, while the Ewald simulation method is applied to compute electrostatic interactions. Fig. 11 illustrates the final equilibrium configurations of the molecular models for solvent-visbroken VR, solvent, saturate, aromatic, resin, and asphaltene at a temperature of 503 K and a pressure of 40 MPa. These configurations are obtained through molecular dynamics simulations conducted under both NPT and NVT ensembles.

Table 8
The molecular distribution of solvent and SARA fraction models.

Solvent model		**Aromatic model**	
n-pentane	300	PHPN	30
Saturate model		DOCHN	30
Squalane	30	**Resin model**	
Hopane	30	Quinolinohopane	7
Asphaltene model		Thioisorenieratane	7
Phenol	15	Benzobisbenzothiophene	26
Pyrrole	10	Pyridinohopane	7
Thiophene	10	Trimethylbenzeneoxane	10

The density variations of visbroken vacuum residue (at 293 K and atmospheric pressure) and n-pentane (at 469.7 K and 3.37 MPa) during molecular dynamics (MD) simulations are plotted in Fig. 12**(a)**. The visbroken vacuum residue reaches equilibrium more rapidly (approximately 40 ps) compared to n-pentane (70 ps), This faster stabilization is attributed to the heavier molecular weight and lower simulation temperature of the visbroken vacuum residue. Additionally, these factors contribute to its higher density relative to n-pentane. The predicted density of visbroken vacuum residue is approximately 1.00 g/cm^3, which closely matches the experimental value of 1.01 g/cm^3. Similarly, the simulated density of n-pentane at 469.7 K (196.5 °C) is around 0.45 g/cm^3, in good agreement with the measured value of 0.432 g/cm^3 [44].

The solubility parameter (δ) components of visbroken vacuum residue and n-pentane at equilibrium are calculated using **Eq.5** and shown in Fig. 12**(b)**. The δ index consists of Van der Waals (Vdw) and electrostatic (Elec) contributions, with the majority arising from Vdw interactions. The predicted δ values for visbroken vacuum residue and n-pentane are 17.74 and 9.15 $(J{\cdot}cm^3)^{0.5}$, respectively, which align well with the corresponding measured values [44,45]. These results confirm the reliability of the molecular model of visbroken vacuum residue and the MD simulation setup employed in this study.

Table 7
The SARA fractions in a molecular model of visbroken vacuum residue.

Chemical fractions	Molecular structure	Chemical formula	Molecule number	Fraction weight (in the model)	Fraction weight (in visbroken vacuum residue)
Saturate	Squalane	$C_{30}H_{62}$	6	14.40 %	14.44 %
	Hopane	$C_{35}H_{62}$	6		
Aromatic	PHPN	$C_{35}H_{44}$	20	46.10 %	46.28 %
	DOCHN	$C_{30}H_{46}$	20		
Resin	Quinolinohopane	$C_{40}H_{59}N$	3	26.40 %	26.08 %
	Thioisorenieratane	$C_{40}H_{60}SO$	3		
	Benzobisbenzothiophene	$C_{18}H_{10}S_2O$	11		
	Pyridinohopane	$C_{36}H_{57}N$	3		
	Trimethylbenzeneoxane	$C_{29}H_{50}O$	4		
Asphaltene	Asphaltene-phenol	$C_{42}H_{54}O$	3	13.10 %	13.20 %
	Asphaltene-pyrrole	$C_{66}H_{81}N$	2		
	Asphaltene-thiophene	$C_{51}H_{62}S$	2		

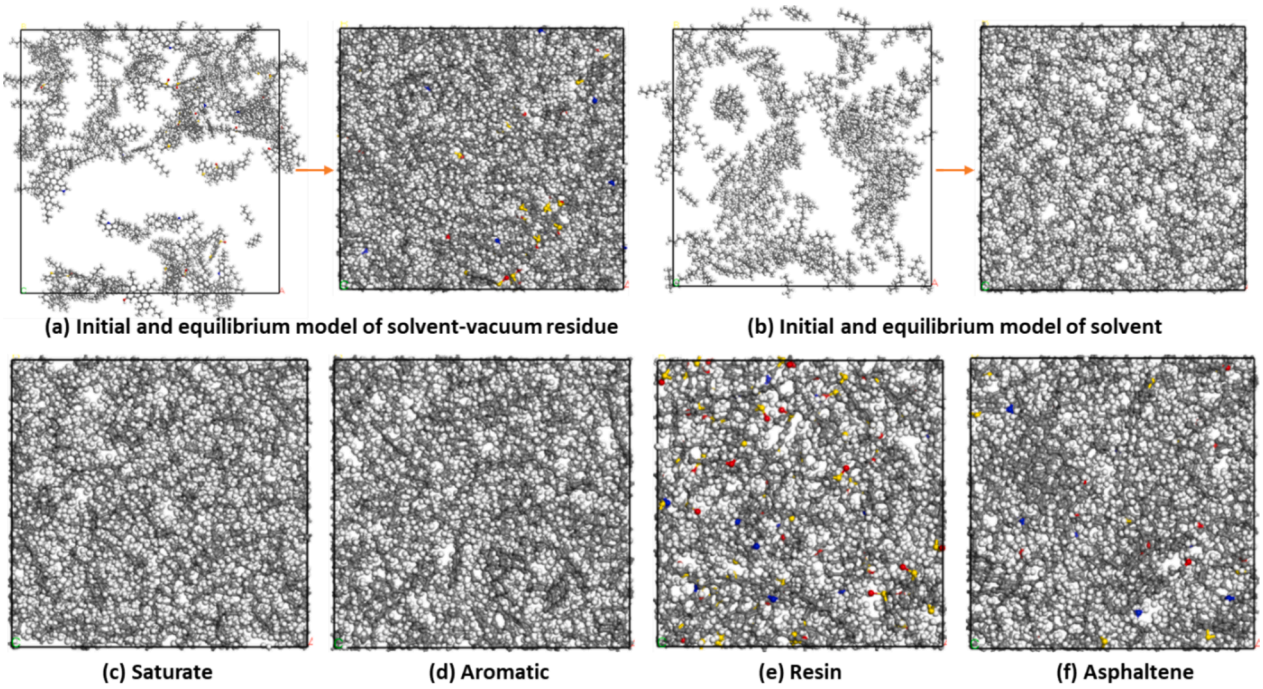

Fig. 11. Molecular models of visbroken vacuum residue and its SARA fractions in the presence of solvent.

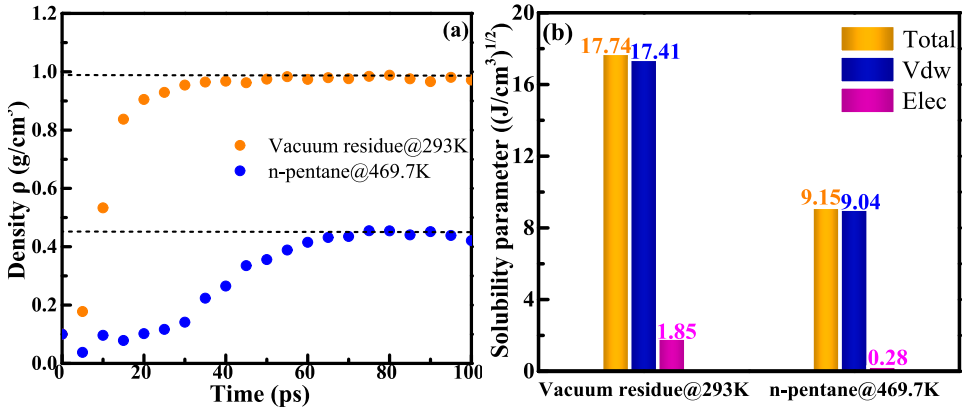

Fig. 12. Density variation and solubility parameter distribution of visbroken vacuum reside and solvent.

$$\delta = (E_{CED})^{1/2} = \left(\frac{E_{coh}}{V}\right)^{1/2} = (E_{vdw} + E_{ele})^{1/2} \quad (5)$$

where E_{CED} represents the cohesive energy density (J/cm^3), which quantifies the overall molecular interactions within a unit volume. E_{coh} (J) denotes the total cohesive energy, while V (cm^3) is the total system volume. Moreover, E_{vdw} and E_{ele} correspond to the cohesive energy density components attributed to van der Waals and electrostatic interactions, respectively.

5.3. Compatibility potential between visbroken vacuum residue and solvent

According to Flory-Huggins theory, materials with similar solubility parameter values are more likely to be miscible. The solubility parameter difference plays a crucial role in determining the compatibility between different components in a compound system [42]. To evaluate the compatibility between different components in a composite system, the solubility parameter difference (Δδ) serves as an effective index. However, Δδ is influenced by external factors such as temperature and pressure. To enhance the compatibility between visbroken vacuum residue and n-pentane, the effects of pressure and temperature on their solubility parameters are investigated using molecular dynamics (MD) simulations. The resulting solubility parameter (δ) values are presented in Fig. 13. Across all temperature and pressure conditions, the δ values of visbroken vacuum residue (VR) remain higher than those of the solvent due to its heavier molecular composition. For both visbroken VR and n-pentane, δ values decrease with increasing temperature, primarily due to weakened intermolecular interactions at elevated temperatures. In contrast, increasing pressure has a positive effect on δ values, with the enhancement being more pronounced for n-pentane than for visbroken VR.

As illustrated in Fig. 13**(c)**, higher pressure significantly reduces Δδ values, indicating improved compatibility and intermolecular interactions between visbroken vacuum residue and n-pentane under supercritical conditions. However, in most cases, Δδ gradually increases with rising temperature. These findings suggest that maintaining a low extraction temperature (above the supercritical threshold) and applying high pressure (within a safe operational range) are beneficial for improving the compatibility and solubility of visbroken vacuum residue

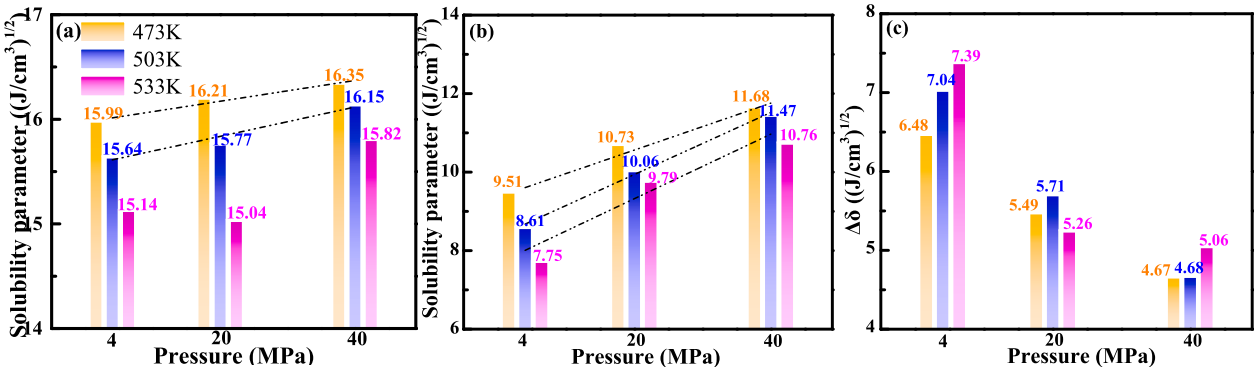

Fig. 13. The solubility parameters of visbroken VR (a) and solvent (b) and their Δδ values (c).

in n-pentane, ultimately enhancing extraction yields.

Table 9 summarizes the solubility parameter (δ) values of the saturate (S), aromatic (A), resin (R), and asphaltene (As) fractions in visbroken vacuum residue under various supercritical temperature and pressure. The results indicate that the heavier components, namely resin and asphaltene, exhibit higher δ values than the lighter fractions, such as aromatic and saturate, across all conditions studied. This suggests that chemical composition significantly influences solubility parameters. For all SARA fractions, δ values decrease with increasing supercritical temperature but increase with rising pressure. However, their sensitivities to temperature and pressure variations differ. To further illustrate these differences, the Δδ values between the SARA fractions and the solvent are depicted in Fig. 14. Due to the molecular similarities between n-pentane and saturate, the corresponding Δδ values are the smallest, followed by aromatic, resin, and asphaltene. This indicates that saturate has the highest dissolution potential in the supercritical solvent. Increasing temperature leads to a rise in Δδ, reducing compatibility, whereas higher pressure enhances the interaction between the solvent and SARA fractions in visbroken vacuum residue. Notably, even under high-pressure conditions (e.g., 40 MPa), the Δδ values of heavy components such as resin and asphaltene remain larger than those of lighter components (saturate and aromatic) under low-pressure conditions (e.g., 4 MPa). It suggests that molecular characteristics, including variations in molecular weight and polarity, have a more significant impact on solubility in the SFE solvent than external conditions such as pressure.

Additionally, the negative impact of temperature on the solubility potential of SARA molecules in the SFE solvent becomes more pronounced under low-pressure conditions. At a high pressure of 40 MPa, the optimal temperature for minimizing Δδ values between the solvent and saturate, aromatic, and resin is observed at 503 K. However, even at elevated pressures, increasing temperature continues to have a detrimental effect on the solubility of asphaltene molecules in the solvent. Thus, to maximize the extraction of light components (saturate and aromatic) while minimizing heavy fractions (resin and asphaltene) in DAO, the optimal SFE conditions within the selected parameter range are 503 K and 40 MPa.

Table 9
Solubility parameter variations of SARA fractions in visbroken vacuum residue.

Pressure	473 K	503 K	533 K	473 K	503 K	533 K
Saturate				**Aromatic**		
4 MPa	13.69	12.99	12.65	15.38	15.47	15.07
20 MPa	13.92	13.38	13.18	15.93	15.37	15.27
40 MPa	14.35	13.89	13.59	16.51	15.73	15.22
Resin				**Asphaltene**		
4 MPa	17.26	17.25	16.90	16.03	15.95	15.75
20 MPa	17.90	17.06	16.86	16.30	15.98	15.53
40 MPa	18.11	17.31	17.00	16.27	16.43	15.88

5.4. Binding energy analysis

At the atomic level, solubility is primarily determined by the strength of intermolecular interactions. Binding energy serves as a key indicator of these interactions within a solution system, with higher binding energy corresponding to stronger intermolecular forces [46]. The binding energy $E_{binding}$ is calculated as follows.

$$E_{binding} = E_A + E_B - E_{A+B} \quad (6)$$

where E_A and E_B denotes the potential energy of molecules A and B, and the E_{A+B} refers to the total potential energy of the solution system.

The binding energy values between the solvent, visbroken vacuum residue, and SARA fractions under varying temperatures and pressures are presented in Fig. 15. The results indicate that SFE pressure and temperature have a significant impact on the binding energy between the solvent and visbroken vacuum residue. Specifically, binding energy increases linearly with pressure, while higher temperatures lead to a reduction in binding energy. This suggests that intermolecular interactions between visbroken vacuum residue and the solvent are stronger at higher SFE pressures and lower temperatures. Furthermore, temperature also influences the rate at which binding energy changes with pressure. As the temperature increases from 473 K to 503 K and 533 K, the slope of the correlation between binding energy and pressure decreases from 0.815 to 0.624 and 0.389, respectively. This trend implies that the positive effect of pressure on intermolecular interactions between the solvent and visbroken vacuum residue weakens as temperature rises.

Fig. 15**(b) and (c)** illustrate the binding energy between the solvent and SARA fractions under varying SFE pressure and temperature conditions. Regardless of the operating conditions, the aromatic fraction exhibits the highest binding energy, indicating the strongest intermolecular interactions with the solvent. Additionally, the binding energy between the solvent and resin is higher than that of saturate and asphaltene. Notably, the effects of SFE pressure and temperature on different SARA fractions vary. For aromatic molecules, binding energy increases with rising pressure but decreases with increasing temperature, a trend consistent with that observed for visbroken vacuum residue. However, the resin fraction exhibits the opposite trend, where low pressure and high temperature enhance its binding energy with the solvent. For saturate molecules, the optimal condition for maximum binding energy is observed at 20 MPa and 533 K. In contrast, asphaltene molecules exhibit the weakest binding energy, reaching their peak value at 4 MPa and 473 K. Thus, the aromatic fraction plays a pivotal role in determining the intermolecular interactions between the solvent and visbroken vacuum residue, while the binding energy index serves as a valuable guide for selecting high-efficiency solvents.

The effects of pressure and temperature on the binding energy

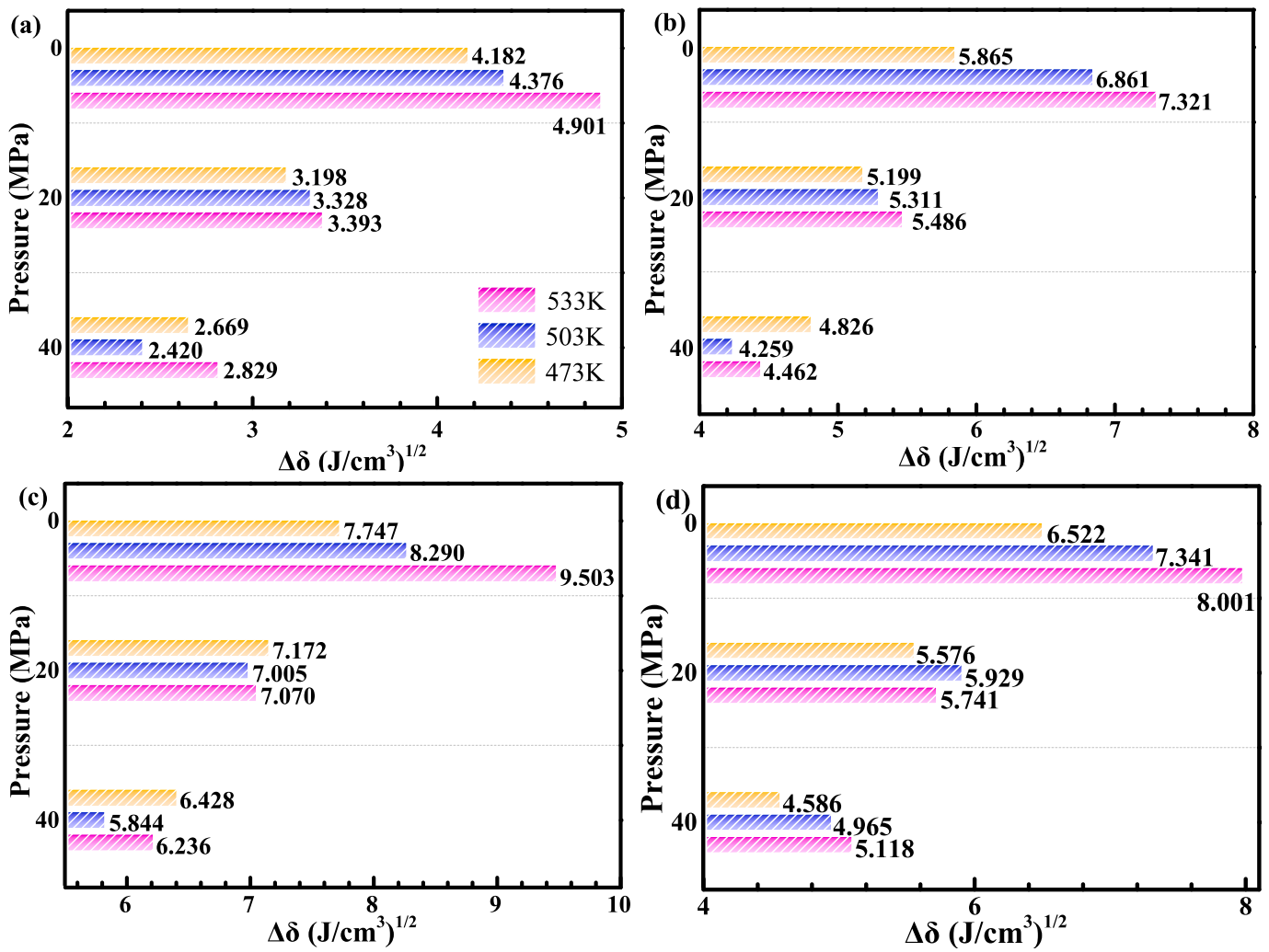

Fig. 14. Solubility parameter difference between solvent and SARA fractions in visbroken vacuum residue. (a) Saturate, (b) Aromatic, (c) Resin, (d) Asphaltene.

between SARA molecules are shown in Fig. 15**(d) and (e)**, respectively. Under all SFE pressure and temperature conditions, the binding energy between the aromatic (A) and the resin-asphaltene (RAs) is the highest. This indicates that separating the aromatic fraction from the resin-asphaltene system is challenging due to the strong adsorption of the aromatic molecules within the colloidal structure. During the SFE process, the binding energy between the resin (R) and asphaltene (As) is the lowest, followed by the interaction between aromatic-resin (AR) and asphaltene (As). This suggests that asphaltene molecules have the highest separation potential under high pressure and temperature conditions, which is consistent with findings of asphaltene molecules tending to agglomerate and undergo phase separation [47]. Furthermore, the binding energy values between the saturate (S) and aromatic-resin-asphaltene (ARAs) fractions, as well as between aromatic (A) and resin (R), are similar, both approaching 600 kcal/mol. Pressure and temperature have minimal impact on the binding energy between SARA fractions. As pressure increases, the binding energy between S-(ARAs) and A-(RAs) shows a slight increase, while the binding energy between R-As and (AR)-As decreases. This suggests that higher SFE pressure favours the separation of aromatic and resin fractions from the colloidal structure. Conversely, as temperature rises, the binding energy of S-(ARAs) decreases, while the binding energy of A-R and A-(RAs) increases. This implies that high temperatures facilitate the separation of the saturate fraction from the others, while enhancing the interaction of the aromatic fraction with resin and asphaltene. Consequently, high temperatures negatively affect the separation of the aromatic fraction and the solubility of the vacuum residue in the solvent. For both the R-As and (AR)-As systems, the binding energy reaches its peak at 503 K, with higher or lower temperatures promoting the separation of asphaltene from the colloidal structure of the visbroken vacuum residue. In conclusion, high pressure enhances the separation of aromatic and resin fractions from the colloidal structure, while high temperature promotes the separation of the saturate fraction, although it negatively affects the solubility and separation of the aromatic fraction from the resin and asphaltene components.

5.5. Diffusion behavior of solvent and visbroken vacuum residue components

In addition to solubility potential and intermolecular interactions, the molecular motion of both the solvent and visbroken vacuum residue molecules can significantly influence the SFE extraction rate [42]. Therefore, the diffusion behavior of the solvent within visbroken vacuum residue is investigated at the atomic level. The equilibrium molecular models are further subjected to the MD simulation with the NVT ensemble for 200 ps, and the mean square displacement (MSD) values variation of solvent-visbroken VR models at different temperatures (473 K, 503 K, 533 K) and pressures (4 MPa, 20 MPa, and 40 MPa) are recorded as the function of simulation time, shown as **Eq.7**. Meanwhile, the self-diffusion coefficient D can be calculated using **Eq.8**.

$$\mathrm{MSD(t)} = < \Delta \mathbf{r}_i(t)^2 > = < [\mathbf{r}_i(t) - \mathbf{r}_i(0)]^2 > \quad (7)$$

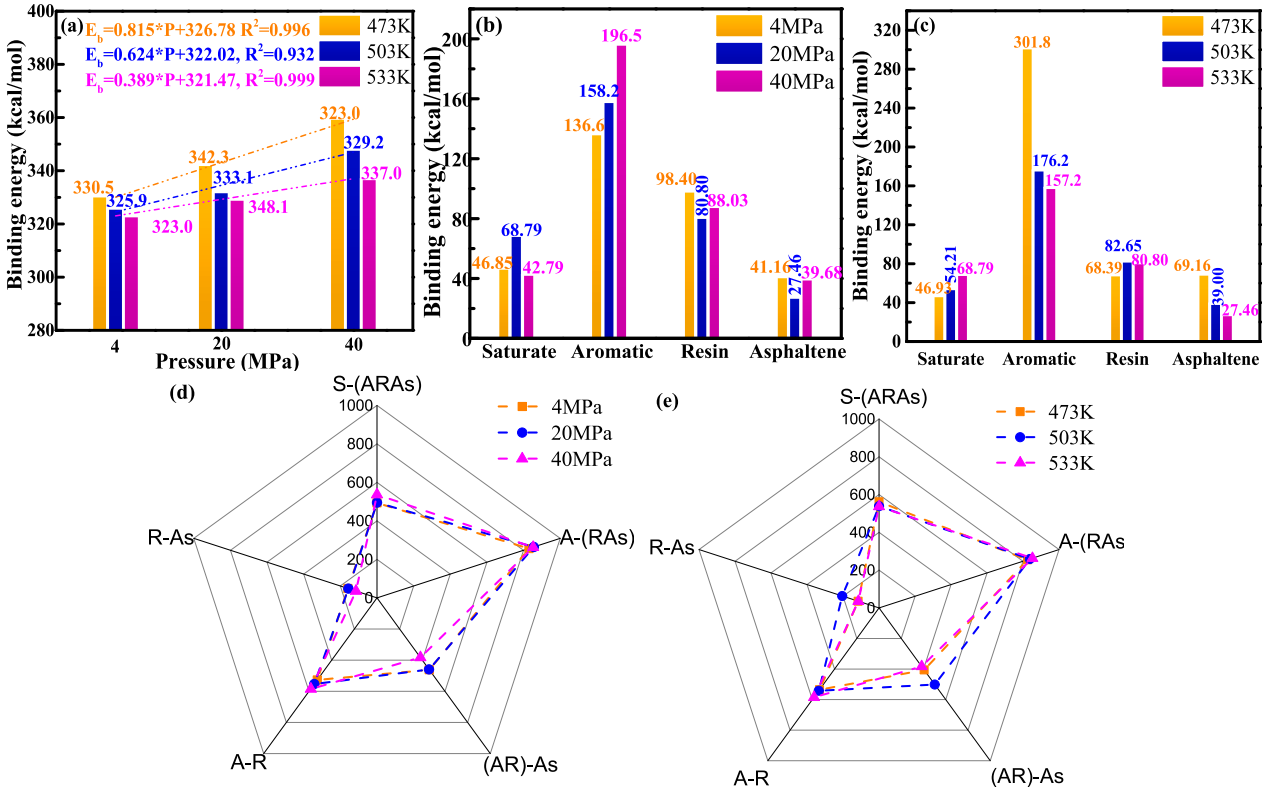

Fig. 15. Binding energy between the solvent and visbroken vacuum residue (SARA fractions).

$$D = \frac{1}{6N}\lim_{t\to\infty}\frac{d}{dt}\sum MSD(t) = \frac{a}{6} \quad (8)$$

where MSD(t) represents the mean square displacement of molecules over time t, and $r_i(0)$ and $r_i(t)$ denote the initial and final coordinates of a molecule at time t, respectively. N is the total number of molecules in the system, and the parameter a corresponds to the slope of correlation curve between MSD and simulation time.

Fig. 16 illustrates the MSD and diffusion coefficient (D) results for the visbroken vacuum residue (VR), its SARA fractions, and the solvent (n-pentane). As anticipated, the MSD values of all molecules increase linearly with simulation time, reflecting the continuous dynamic motion of the molecules. The MSD-t correlation equations for the total system, visbroken vacuum residue, and solvent are shown in Fig. 16**(a)**. Notably, the MSD values of the solvent are significantly higher than those of the visbroken vacuum residue, which can be attributed to the lower molecular weight and non-polar nature of the n-pentane molecules. The large slope of the MSD-t curve indicates the high diffusion capacity of

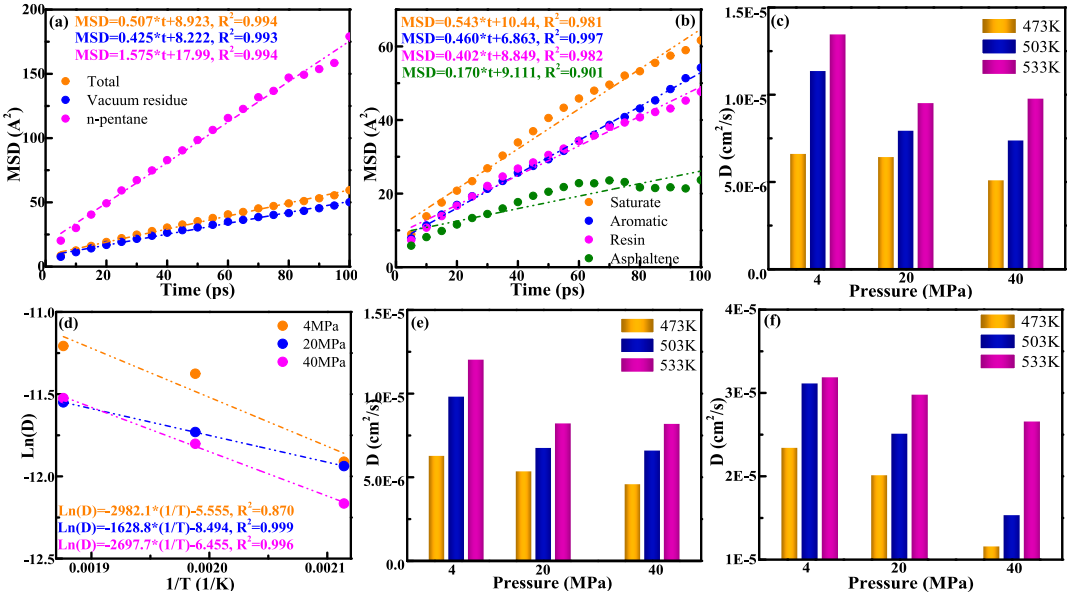

Fig. 16. MSD and D values of visbroken vacuum residue, SARA fractions and solvent. (a) MSD of blend, visbroken VR and n-pentane; (b) MSD of SARA fractions in visbroken VR; (c) D of solvent-visbroken VR; (d) D-T curve of solvent-visbroken VR; (e) D of visbroken VR; (f) D of solvent.

the solvent molecules. Fig. 16**(b)** compares the MSD-t curves for the SARA fractions in visbroken vacuum residue within the solvent environment. The saturate molecules exhibit the highest MSD values, followed by aromatic and resin fractions, while the asphaltene fraction shows the lowest MSD values. This indicates that the diffusion capacity of the SARA fractions follows the order: saturate > aromatic > resin > asphaltene. Additionally, the saturate molecules diffuse more slowly than the solvent. The diffusion capacity of solvent-visbroken VR molecules is significantly influenced by temperature and pressure. As the temperature (T) increases, the self-diffusion coefficient (D) values for all molecules rise due to the additional energy gained. A linear relationship between Ln(D) and 1/T for the SFE model is observed, which is also affected by the pressure. As pressure increases, the temperature sensitivity of the D parameter initially decreases then increases.

However, the effect of pressure on the self-diffusion coefficient (D) of SFE molecules varies with temperature. At lower temperatures (473 K and 503 K), increasing pressure leads to a decline in D values, including that high pressure reduces the diffusion rate of SFE molecules, providing them with more time to interact with visbroken vacuum residue molecules, thereby enhancing the extraction yield. At higher temperature (533 K), D values decrease as pressure increases from 4 MPa to 20 MPa but then rise when pressure further increases to 40 MPa. A similar trend is observed for visbroken vacuum residue, as shown in Fig. 16**(e)**. In contrast, for the solvent, increasing pressure consistently results in a decrease in D values, suggesting a general suppression of solvent diffusion under high-pressure conditions.

To further investigate the impact of pressure on the diffusion behaviour of visbroken vacuum residue components, the self-diffusion coefficient (D) results of saturate, aromatic, resin, and asphaltene molecules are plotted in Fig. 17. Across all SARA fractions, the D values progressively decrease with increasing pressure under all temperature conditions, indicating that elevated pressure impairs the molecular diffusively of visbroken vacuum residue components. Additionally, a linear correlation is observed between the D parameter and the logarithmic value of pressure for all SARA molecules, with the corresponding correlation equations provided. The sensitivity of D values for SARA fractions varies with temperature. As temperature increases, the pressure sensitivity of the D index for aromatic molecules gradually decreases, suggesting that the negative impact of pressure of their diffusivity diminishes at higher temperatures. Similarly, the pressure sensitivity trends for saturate and resin fractions follow a pattern of initial increase followed by a decline. In contrast, the asphaltene fraction exhibits the opposite behavior, indicating a distinct response to pressure and temperature variations.

On the other hand, the temperature sensitivity of D values at different pressure levels for visbroken vacuum residue, solvent, and SARA fractions is also investigated, and the results are depicted in Fig. 18. The Arrhenius equation is adopted to quantitatively investigate the pressure level on the relationship between diffusion coefficient and temperature as shown below:

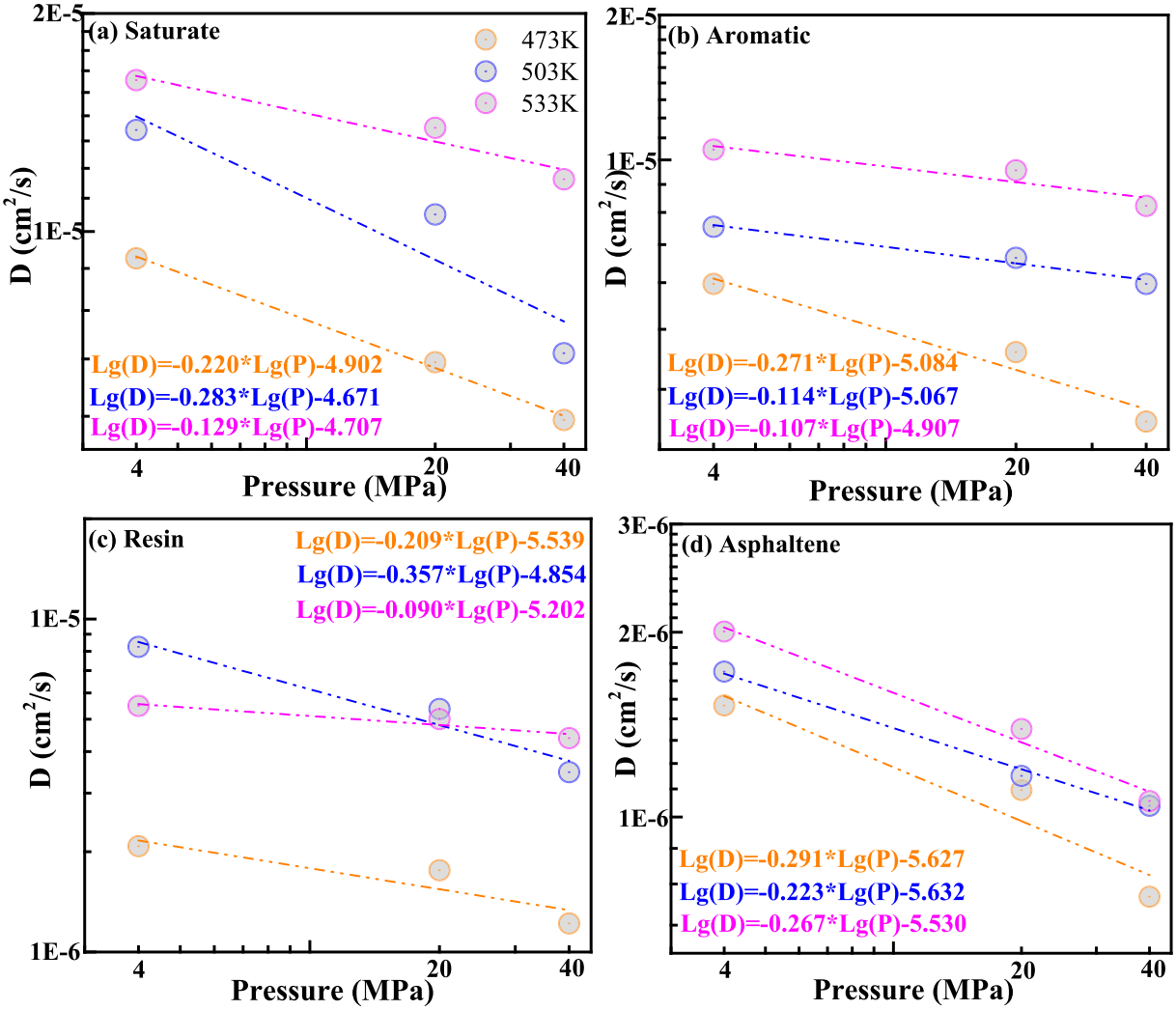

Fig. 17. D variations of SARA fractions under different temperature and pressure conditions.

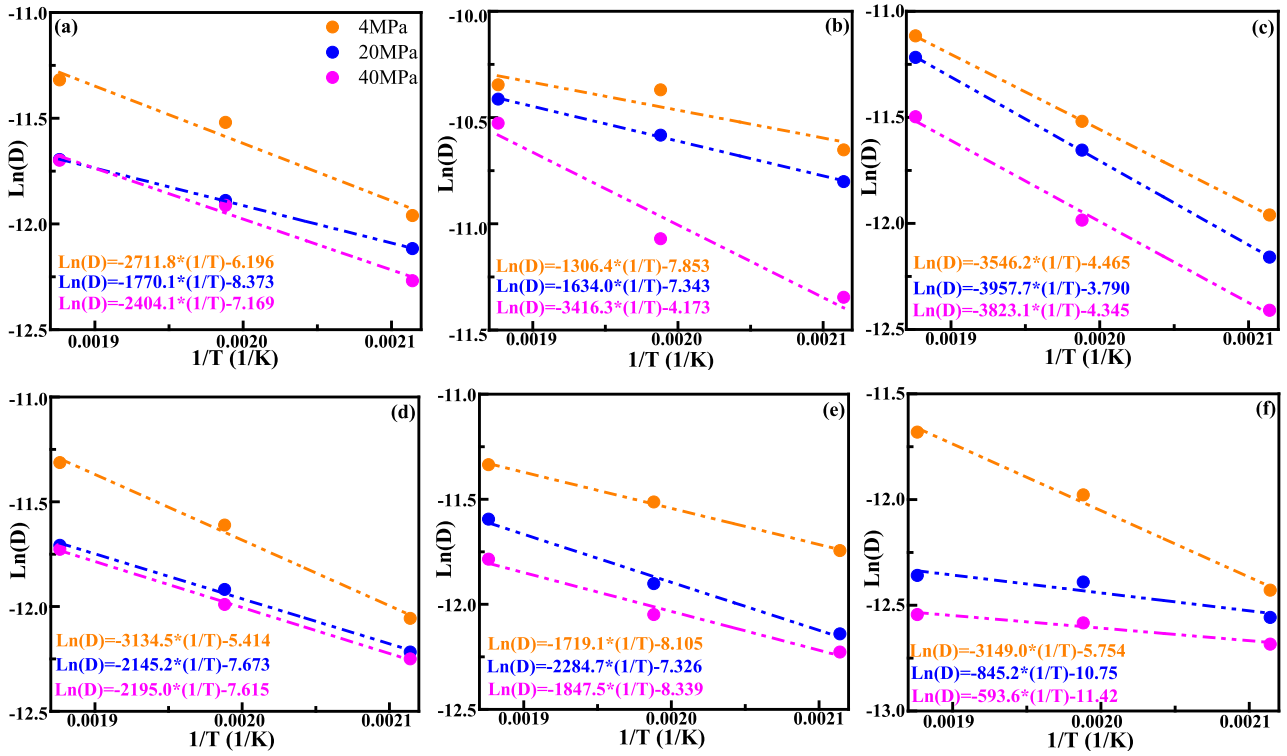

Fig. 18. Effect of temperature on self-diffusion capacity of visbroken vacuum residue (a), solvent (b), saturate (c), aromatic (d), resin (e), and asphaltene (f).

$$D = D_0 \exp\left(\frac{-E_D}{RT}\right) \quad (9)$$

where R denotes the universal gas constant (8.314 J/mol·K^{-1}), E_D is the experimental activation energy per mol, and Do is the frequency factor and is taken as practically independent of temperature T.

The linear correlations between Ln(D) and 1/T for all models confirm that the diffusivity of visbroken VR, solvent, and SARA fractions decreases with increasing pressure. Additionally, a lower temperature (higher 1/T) further reduces D values. Thus, high temperatures and low pressures enhance the diffusion rates of solvent and visbroken vacuum residue molecules, increasing their collision probability [40]. Moreover, pressure significantly influences the decreasing rate in Ln(D) versus 1/T. Based on the absolute slope values of the correlation equations, higher pressure increases the temperature sensitivity of solvent molecules but reduces that of asphaltene molecules. At 20 MPa, visbroken vacuum residue and aromatic fraction exhibit the lowest temperature sensitivity, whereas the resin fraction shows the highest sensitivity. For saturate molecules, the effect of pressure on temperature sensitivity remains minimal because of its sufficient diffusive capacity.

The activation energy E_D and pre-exponential factor D_0 of visbroken vacuum residue, solvent, and SARA fractions are calculated using **Eq.9** and summarized in Table 10. The results indicate that E_D values generally decrease with increasing pressure for most components, suggesting that higher pressures hinder molecular diffusion by reducing the energy required for molecular movement. Among the SARA fractions, the saturate fraction exhibits the highest E_D values across all pressures, implying greater sensitivity to temperature variations, while asphaltene shows the lowest values, indicating a relatively stable diffusion behavior. The solvent (n-pentane) has the lowest E_D among all components, reinforcing its superior diffusivity. Additionally, D_0 values decrease significantly with increasing pressure, particularly for visbroken vacuum residue and solvent, confirming that elevated pressure restricts molecular mobility. Notably, the resin fraction displays an anomaly, with its E_D peaking at 20 MPa before decreasing at 40 MPa, suggesting a complex interaction with pressure. These findings emphasize that pressure exerts a substantial influence on diffusion behavior, with a pronounced restrictive effect at higher pressures, particularly for lighter fractions like solvent and saturate.

6. Conclusions and recommendations

This study investigated the Visbreaking-Supercritical Fluid Extraction (SFE) combination process for the removal of high-carbon compounds and metals from vacuum residue (VR). Comprehensive physical and chemical characterizations were performed on both the feedstock and the resulting fractions to evaluate the effectiveness of this novel chemical extraction process. The efficiency of decarbonization and

Table 10
E_D and D_o parameters of visbroken VR, solvent, and SARA fractions under variable pressures.

Visbroken VR	4 MPa	20 MPa	40 MPa	**Solvent**	4 MPa	20 MPa	40 MPa
E_D (J/mol)	22,546	14,717	19,988	E_D (J/mol)	10,861	13,585	28,403
D_o (cm^2/s)	2.038E-3	2.310E-4	7.701E-4	D_o (cm^2/s)	3.886E-4	6.471E-4	1.541E-2
Saturate	4 MPa	20 MPa	40 MPa	**Aromatic**	4 MPa	20 MPa	40 MPa
E_D (J/mol)	29,483	32,904	31,785	E_D (J/mol)	26,060	17,835	18,249
D_o (cm^2/s)	1.150E-2	2.260E-2	1.297E-2	D_o (cm^2/s)	4.454E-3	4.652E-4	4.930E-4
Resin	4 MPa	20 MPa	40 MPa	**Asphaltene**	4 MPa	20 MPa	40 MPa
E_D (J/mol)	14,293	18,995	15,360	E_D (J/mol)	26,181	7027	4935
D_o (cm^2/s)	3.020E-4	6.582E-4	2.390E-4	D_o (cm^2/s)	3.170E-3	2.145E-5	1.097E-5

demetallizaion was analysed in detail. Additionally, molecular dynamics (MD) simulations provided fundamental insights into the atomic-scale thermodynamic and solubility mechanisms governing the SFE process. The key findings of this work are summarized as follows:

(1) Compared to standalone Visbreaking and SFE processes, the Visbreaking-SFE combination significantly enhances both decarbonization and demetalization. This integrated approach achieves a total liquid yield of up to 70.1 % while effectively removing metals such as Fe, Ni, V, and Na, with removal efficiencies exceeding 62 %, 75 %, and 95 %, respectively.
(2) To produce high-quality DAO products, Visbreaking should operate under mild thermal cracking conditions at relatively low temperatures to prevent premature coke formation. In this study, the optimal Visbreaking conditions for processing Merey VR were identified as a reaction temperature of 400 °C and a reaction time of 40 min. Higher extraction pressures and low extraction temperatures improve DAO recovery but increase metal and sulfur content, requiring a balance between DAO yield and quality.
(3) Molecular dynamics simulations provide atomic-scale insights into interactions between solvent and visbroken vacuum residue fractions, confirming that high pressure and moderate temperatures optimize solubility, diffusion, and binding energy between visbroken vacuum residue components and the supercritical solvent. The binding energy analysis confirms that aromatic fractions have the strongest interaction with the solvent, influencing the yield and selectivity of the SFE process. These insights offer a fundamental understanding of the thermodynamic and kinetic behavior governing the upgrading process, guiding future optimization efforts.
(4) From an industrial and environmental perspective, the extracted DAO meets marine fuel specifications, ensuring compliance with stringent sulfur and metal content regulations. Meanwhile, the raffinates can be repurposed for bitumen production, either as modifiers or substitutes for traditional bitumen, expanding their application in sustainable construction materials. The Visbreaking-SFE approach offers a scalable, cost-effective, and environmentally friendly solution for upgrading low-quality heavy residues, aligning with the petroleum industry's shift toward cleaner, more sustainable refining technologies.

Future research should focus on optimizing solvent selection and process conditions to maximize DAO yield while minimizing energy consumption and solvent losses. Investigating alternative solvents or solvent mixtures with improved selectivity for different VR fractions could further refine the extraction process. Additionally, another future work will explore phase separation behavior of solvent-visbroken VR system under supercritical conditions through an integrated approach combining extended MD simulations with continuum-scale COMSOL modelling, to provide a direct comparison with SFE experimental data. Lastly, exploring the potential of the extracted fractions beyond marine fuel and bitumen applications, such as in petrochemical feedstocks or advanced carbon materials, could further enhance the economic viability and sustainability of this Visbreaking-SFE process during the industrial applications.

CRediT authorship contribution statement

Shisong Ren: Methodology, Investigation, Formal analysis, Writing – original draft. **Ying He:** Investigation, Writing – review & editing. **Cheng Liu:** Writing – review & editing. **Weiyu Fan:** Supervision, Methodology, Software, Writing – review & editing. **Wim Van den bergh:** Methodology, Supervision, Writing – review & editing. **Aikaterini Varveri:** Supervision, Writing – review & editing.

Declaration of competing interest

The authors declare that they have no known competing financial interests or personal relationships that could have appeared to influence the work reported in this paper.

Acknowledgements

The first author, Shisong Ren, would appreciate the funding supports from the Research Foundation-Flanders (FWO, Belgium) with postdoc fellowship [No. 1202125 N] and from the European Commission with Horizon Europe Programme under the Marie Skłodowska-Curie grant agreement [No. 101203557].

Data availability

Data will be made available on request.

References

[1] L. Castaneda, J. Munoz, J. Ancheyta, Current situation of emerging technologies for upgrading of heavy oils, Catal. Today 220–222 (3) (2014) 248–273.
[2] Y. Xi, Z. Shao, Y. Sun, W. Teng, S. Zhang, J. Yang, Z. Huang, J. Gong, P. Yuan, Continuous visbreaking of heavy oil in medium and high-pressure steam environments, J. Anal. Appl. Pyrol. 179 (2024) 106475.
[3] J. Joshi, A. Pandit, K. Kataria, R. Kulkarni, A. Sawarkar, D. Tandon, Y. Ram, M. Kumar, Petroleum residue upgradation via visbreaking: a review, Ind. Eng. Chem. Res. 47 (23) (2008) 8960–8988.
[4] J.L. Hedrick, L.J. Mulcahey, L.T. Taylor, Supercritical fluid extraction, Mikrochim. Acta 108 (1992) 115–132.
[5] A.H. Almarzouqi, M.V. Rao, B. Jobe, Comparative evaluation of SFE and steam distillation methods on yield and composition of essential oil extracted from spearmint (Mentha spicata), J. Liq. Chromatogr. Relat. Technol. 30 (4) (2007) 463–475.
[6] Y. Yan, A. Klerk, G. Prado, Visbreaking of vacuum residue deasphalted oil: new asphaltenes formation, Energy Fuel 34 (2020) 5135–5147.
[7] E. Yabalak, M.A. Gizir, Subcritical and supercritical fluid extraction of heavy metals from sand and sewage sludge, J. Serb. Chem. Soc. 78 (7) (2013) 1013–1022.
[8] J.Q. Albarelli, R.B. Rabelo, D.T. Santos, M.M. Beppu, M.A. Meireles, Effects of supercritical carbon dioxide on waste banana peels for heavy metal removal, J. Supercrit. Fluids 58 (3) (2011) 343–351.
[9] M.F. Ali, S. Abbas, A review of methods for the demetallization of residual fuel oils, Fuel Process. Technol. 87 (7) (2006) 573–584.
[10] T. Shi, Y. Hu, Z. Xu, T. Su, R. Wang, Characterization petroleum vacuum residue by supercritical fluid extraction and fraction, Ind. Eng. Chem. Res. 36 (9) (1997) 3988–3992.
[11] J. Lee, S. Shin, S. Ahn, J. Chun, K. Lee, S. Mun, S. Jeon, J. Na, N. Nho, Separation of solvent and deasphalted oil for solvent deasphalting process, Fuel Process. Technol. 119 (2014) 204–210.
[12] J. Cheng, Y. Fan, Y. Zhan, Supercritical propane fractionation of wax-bearing residue, Sep. Sci. Technol. 29 (14) (1994) 1779–1787.
[13] T. Shi, Z. Xu, M. Cheng, Y. Hu, R. Wang, Characterization index for vacuum residua and their subfractions, Energy Fuel 13 (4) (1999) 871–876.
[14] S. Zhao, Z. Xu, C. Xu, K.H. Chung, R. Wang, Systematic characterization of petroleum residua based on SFEF, Fuel 84 (6) (2005) 635–645.
[15] L. Zhang, Z. Xu, Q. Shi, X. Sun, N. Zhang, Y. Zhang, S. Zhao, Molecular characterization of polar heteroatom species in Venezuela Orinoco petroleum vacuum residue and its supercritical fluid extraction subfractions, Energy Fuel 26 (9) (2012) 5795–5803.
[16] H. Li, Q. Chang, Z. Dai, X. Chen, G. Yu, F. Wang, Upgrading effects of supercritical carbon dioxide extraction on physicochemical characteristics of Chinese low-rank coals, Energy Fuel 31 (12) (2017) 13305–13316.
[17] X. Lin, S. Li, F. Guo, G. Jiang, X. Chen, Y. Wang, High-efficiency extraction and modification on the coal liquefaction residue using supercritical fluid with different types of solvents, Energy Fuel 30 (5) (2016) 3917–3928.
[18] S.A. Brough, S.H. Riley, G.S. Mcgrady, S. Tanhawiriyakul, L. Romerozeron, C. Willson, Low temperature extraction and upgrading of oil sands and bitumen in supercritical fluid mixtures, Chem. Commun. 46 (27) (2010) 4923–4925.
[19] D.S. Scott, D. Radlein, J. Piskorz, P. Majerski, T.J. Debruijn, Upgrading of bitumen in supercritical fluids, Fuel 80 (8) (2001) 1087–1099.
[20] J. Wang, K. Tian, Y. Li, W. Wang, H. Jin, Diffusion coefficients of polycyclic aromatic hydrocarbons in supercritical carbon dioxide: a molecular dynamics simulation study, J. Mol. Liq. 409 (2024) 125457.
[21] J. Wang, M. Guan, J. Zhang, H. Jin, Molecular dynamics simulation of polycyclic aromatic hydrocarbons solvation behavior in supercritical carbon dioxide under different pressure and temperature, J. Supercrit. Fluids 208 (2024) 106233.
[22] F. Simeski, M. Ihme. Supercritical fluids behave as complex networks. Nature Communications. https://doi.org/10.1038/s41467-023-37645-z.
[23] J. Park, K. Lee, Molecular dynamics simulations of asphaltene aggregation in heavy oil system for the application to solvent deasphalting, Fuel 323 (2022) 124171.

[24] J. Park, M. Kim, S. Im, K. Go, N. Nho, K. Lee, Development of correlations between deasphalted oil yield and Hansen solubility parameters of heavy oil SARA fractions for solvent deasphalting extraction, J. Ind. Eng. Chem. 107 (2022) 456–465.
[25] L.C. Castañeda, J.A.D. Muñoz, J. Ancheyta, Combined process schemes for upgrading of heavy petroleum, Fuel 100 (100) (2012) 110–127.
[26] C. Ma, G. Li, J. Zhang, Q. Zheng, X. Fan, Z. Wang, An efficient combination of supercritical fluid extraction and high-speed counter-current chromatography to extract and purify homoisoflavonoids from Ophiopogon japonicus (Thunb.) Ker-Gawler, J. Sep. Sci. 32 (11) (2009) 1949–1956.
[27] A.P. Sanchezcamargo, F. Paradaalfonso, E. Ibanez, A. Cifuentes, On-line coupling of supercritical fluid extraction and chromatographic techniques, J. Sep. Sci. 40 (1) (2017) 213–227.
[28] ASTM D1480-21. Standard Test Method for Density and Relative Density (Specific Gravity) of Viscous Materials by Bingham Pycnometer. 2021. DOI: 10.1520/D1480-21.
[29] ASTM D445-21. Standard Test Method for Kinematic Viscosity of Transparent and Opaque Liquids (and Calculation of Dynamic Viscosity). 2021. DOI: 10.1520/D0445-21E01.
[30] ASTM D7679-16. Standard Test Method for Sulfur Content in Carbon Black Feedstock Oils. 2020. DOI: 10.1520/D7679-16R20.
[31] ASTM D189-06. Standard Test Method for Conradson Carbon Residue of Petroleum Products. 2019. DOI: 10.1520/D0189-06R19.
[32] ASTM D4072-98. Standard Test Method for Toluene-Insoluble (TI) Content of Tar and Pitch. 2018. DOI: 10.1520/D4072-98R18.
[33] ASTM D4055-04. Standard Test Method for Pentane Insolubles by Membrane Filtration. 2019. DOI: 10.1520/D4055-04R19.
[34] STP11992S. Direct Trace and Ultra-Trace Metals Determination in Crude Oil and Fractions by Inductively Coupled Plasma Mass Spectrometry.
[35] Z. Wang, Z. Cui, Determination of arsenic species in solid matrices utilizing supercritical fluid extraction coupled with gas chromatography after derivatization with thioglycolic acid n-butyl ester, J. Sep. Sci. 39 (23) (2016) 4568–4576.
[36] M. Liu, L. Zhang, S. Zhao, D. Zhao, Transformation of nitrogen compounds through hydrotreatment of Saudi Arabia atmospheric residue and supercritical fluid extraction subfractions, Energy Fuel 30 (1) (2016) 740–747.
[37] O. Omole, M.N. Olieh, T. Osinowo, Thermal visbreaking of heavy oil from the Nigerian Tar sand, Fuel 78 (1999) 1489–1496.
[38] P.G. Debenedetti, Supercritical fluid extraction principles and practice, AIChE J. 33 (8) (1987) 1406–1407.
[39] ISO 8217-2017. Fuel Standard for Marine Distillate Fuels.
[40] S. Shin, J. Lee, J. Hwang, H. Jung, N. Nho, K. Lee, Physical and rheological properties of deasphated oil produced from solvent deasphalting, Chem. Eng. J. 157 (2014) 242–247.
[41] D. Li, M. Greenfield, Chemical compositions of improved model asphalt systems for molecular simulations, Fuel 115 (2014) 347–356.
[42] S. Ren, X. Liu, P. Lin, S. Erkens, Y. Xiao, Chemo-physical characterization and molecular dynamics simulation of long-term aging behaviors of bitumen, Constr. Build. Mater. 302 (2021) 124437.
[43] G. Li, Y. Tan, The construction and application of asphalt molecular model based on the quantum chemistry calculation, Fuel 308 (2022) 122037.
[44] M. AI-Sabawi, D. Seth, T. Bruijn, Effect of modifiers in n-pentane on the supercritical extraction of Athabasca bitumen, Fuel Process. Technol. 92 (2011) 1929–1938.
[45] X. Zou, L. Dukhedin-Lalla, X. Zhang, J. Shaw, Selective rejection of inorganic fine solids, heavy metals, and sulfur from heavy oils/bitumen using alkane solvents, Ind. Eng. Chem. Res. 43 (2004) 7103–7112.
[46] S. Ren, X. Liu, P. Lin, Y. Gao, S. Erkens, Insight into the compatibility behaviors between various rejuvenators and aged bitumen: molecular dynamics simulation and experimental validation, Mater. Des. 223 (2022) 111141.
[47] A. Tirjoo, B. Bayati, H. Rezaei, M. Rahmati, Molecular dynamics simulations of asphaltene aggregation under different conditions, J. Pet. Sci. Eng. 177 (2019) 392–402.